

SMR 1331/15

## **AUTUMN COLLEGE ON PLASMA PHYSICS**

8 October - 2 November 2001

# **AURORAL ZONE PLASMA PHYSICS**

**Robert L. Lysak**

**University of Minnesota, U.S.A.**



## Auroral Zone Plasma Physics

Robert L. Lysak, University of Minnesota

### Introduction

The auroral zone can be defined as the magnetic flux tubes that extend upward from the auroral ionosphere, the region at about  $70^\circ$  geomagnetic latitude in both the northern and southern hemispheres. The auroral zone is a fertile region for the study of plasma physics due to a number of its unique characteristics. First of all, the auroral zone is a region in which field-aligned currents flow. A consequence of these field-aligned currents is that parallel electric fields develop in this region. These parallel electric fields appear to be localized in the region around 6000 km altitude, a region called the auroral acceleration region. The reason for these parallel electric fields is still controversial, but nearly all researchers in this area associate them with the field-aligned currents in the auroral zone. In the time-dependent case, the field-aligned currents evolve by the propagation of Alfvén waves along field lines. Ideal MHD Alfvén waves do not carry an electric field and cannot accelerate particles; however, on the small spatial scales present in the auroral zone, these Alfvén waves must be described by kinetic theory, and parallel electric fields can develop. The interaction of these Alfvén waves with the ionosphere can lead to structuring of the field-aligned currents. Another aspect of the auroral zone is that there are strong gradients in the density, temperature, and magnetic field strength along the magnetic field lines. Such gradients can directly affect Alfvén wave propagation as well as higher frequency waves. The strong field-aligned currents imply that there is a relative drift between the electrons and ions in this region that can give rise to instabilities. In addition, the gradients in the magnetic field strength lead to a magnetic mirror force that can strongly affect the particle distributions along auroral field lines by leading to a loss cone in the distributions. Even though the auroral electrons are only weakly relativistic, relativity modifies the cyclotron resonance condition and can give rise to strong radio emissions. These features of the auroral zone make it a fascinating place of study for plasma physicists.

The auroral zone can be characterized as being a strongly magnetized plasma, in which the electron plasma frequency can be much less than the electron gyrofrequency,  $\omega_{pe} \ll \Omega_e$ , and indeed, in some cases we also have  $\omega_{pi} < \Omega_i$ . (These conditions do not apply to the collisional ionosphere, where the density is much higher.) This strong magnetization, or equivalently low plasma density, affects many of the auroral zone properties. The auroral zone plasma is a mixture of cold ionospheric plasma ( $T \sim 1$  eV) and hot magnetospheric plasma ( $T \sim 100$  eV). These population and the strong magnetic field mean that the auroral zone is a low beta ( $\beta = 2\mu_0 p / B^2$ ) plasma. Indeed,  $\beta$  can be extremely low, less than  $10^{-6}$ . As we shall see, this has consequences for the acceleration of auroral particles and the propagation of Alfvén waves.

### A. Parallel electric fields in the auroral zone

#### 1. Response of auroral particles to parallel electric fields

The nearly dipolar magnetic field on these field lines implies that the magnetic mirror force operates on these particles. On the other hand, the field-aligned currents in the ionosphere can lead to the development of parallel potential drops on auroral field lines. We will discuss the mechanisms for these potential drops later, but for now we will assume their existence and ask their effect on the velocity space structure of auroral particles. This velocity space structure can be seen by considering the two invariants of the motion, the total energy and the magnetic moment of the particle (see, e.g., Chiu and Schulz, 1978). Assuming non-relativistic motion to simplify the algebra, the invariants become:

$$E = \frac{1}{2}m(v_{\parallel}^2 + v_{\perp}^2) + q\Phi \quad (1)$$

$$\mu = \frac{mv_{\perp}^2}{2B} \quad (2)$$

These invariants imply that if the particle has a velocity  $v_{\parallel,1}$  and  $v_{\perp,1}$  at a location where the magnetic field and the potential are  $B_1$  and  $\Phi_1$ , then its parallel velocity at a location  $B_2$ ,  $\Phi_2$  is given by:

$$v_{\parallel 2}^2 = v_{\parallel 1}^2 + v_{\perp 1}^2 \left(1 - \frac{B_2}{B_1}\right) - \frac{2q(\Phi_2 - \Phi_1)}{m} \quad (3)$$

Note that the RHS of equation (3) must be greater than zero for the particle to be accessible to point 2.

Let us now consider a situation where the field-aligned current and the parallel electric field point in the upward direction. This implies that the potential increases as one moves downward along the field line. There are two possible sources for plasma on this field line, one being the outer magnetosphere and the other being the ionosphere. The magnetospheric source is generally rather hot, with temperatures of 100-1000 eV and densities less than  $1 \text{ cm}^{-3}$ , while the ionospheric source is much colder, 1-10 eV, but can be much more dense. Let  $B_s$  be the magnetic field in the magnetospheric source, and let  $\Phi_s = 0$  at this point. We will denote the magnetic field and potential in the ionosphere as  $B_I$  and  $\Phi_I$ . Note that magnetospheric particles that reach the ionosphere will collide with ionospheric particles and be lost. We will write quantities at the observation point without any subscripts. Note that we will assume  $B_s < B < B_I$

and  $0 < \Phi < \Phi_I$ .

First, consider ion motion, so that  $q > 0$ . For ions, both the magnetic mirror force and the parallel electric field produce an upward force. For an ion not to be lost into the ionosphere, its parallel velocity must go to zero (where it is reflected) before hitting the ionosphere. This condition can be written as:

$$v_{\parallel I}^2 = v_{\parallel}^2 - v_{\perp}^2 \left(\frac{B_I}{B} - 1\right) - \frac{2q(\Phi_I - \Phi)}{m} < 0 \quad (4)$$

It can be seen that this condition leads to a hyperbola in velocity space that crosses the  $v_{\perp} = 0$  axis at the point  $v_{\parallel}^2 = 2q(\Phi_I - \Phi)/m$ . At very

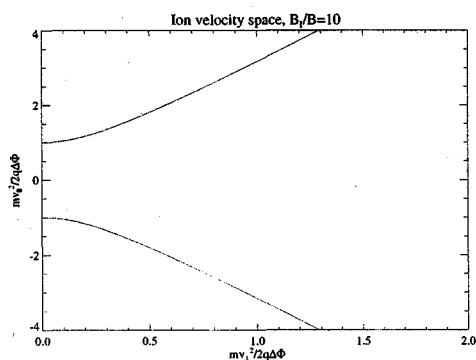


**Figure 1. Ion velocity space structure for an upward parallel electric field.**

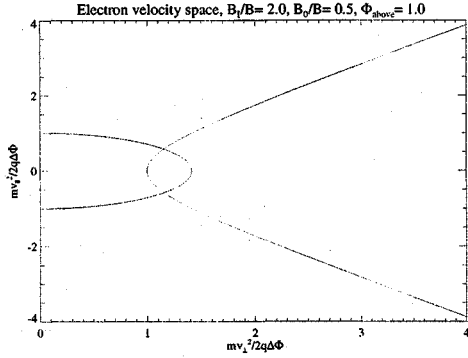


**Figure 2. Electron velocity space for upward parallel electric field.**

large velocities, the term in equation (4) involving the potential drops out, and this hyperbola reduces to the usual loss cone at a pitch angle  $\tan \alpha = v_{\perp} / v_{\parallel} = 1 / (B_t / B - 1)$ . Points inside the hyperbola (i.e., those with greater parallel velocities) will hit the ionosphere and be lost; thus, the upgoing part inside the hyperbola will not contain any magnetospheric particles. On the other hand, ions that originate in the ionosphere can only be present in this upgoing loss cone region, and will form an upgoing beam. Magnetospheric ions outside the hyperbola will reflect before they hit the ionosphere. The velocity space structure for ions is shown in Figure 1.

The situation for electrons with an upward parallel electric field is more complicated. For ions, the electric field and the mirror force point in the same direction; however, for electrons, the mirror force is upward while the force from the parallel electric field is downward, which complicates the velocity space structure. For a magnetospheric electron to avoid loss in the ionosphere, it must satisfy a condition similar to (4) but with  $q = -e$ :

$$v_{\parallel}^2 = v_{\parallel}^2 - v_{\perp}^2 \left( \frac{B_t}{B} - 1 \right) + \frac{2e(\Phi_t - \Phi)}{m} < 0 \quad (5)$$

This still gives a hyperbola, but one which crosses the  $v_{\parallel} = 0$  axis rather than the  $v_{\perp} = 0$  axis as was the case with the ions. In addition, however, not every point in the electron velocity space is accessible from the magnetospheric source. To determine this condition, we can consider a point in velocity space at the observation point and trace its trajectory back to see whether it can reach the source. This procedure leads to the condition:

$$v_{\parallel s}^2 = v_{\parallel}^2 + v_{\perp}^2 \left( 1 - \frac{B_s}{B} \right) - \frac{2e\Phi}{m} > 0 \quad (6)$$

This condition describes the exterior of an ellipse in velocity space, which is sometimes termed the “acceleration ellipse,” which crosses the  $v_{\perp} = 0$  axis at  $v_{\parallel}^2 = 2e\Phi / m$  and crosses the  $v_{\parallel} = 0$  axis at  $v_{\perp}^2 = (2e\Phi / m) / (1 - B_0 / B)$ . The region inside this ellipse is inaccessible for electrons originating in the outer magnetosphere. This velocity space structure is shown in Figure 2.

From this figure it can be seen that there are 5 distinct regions of velocity space. At large parallel velocity and small perpendicular velocity, the downward electrons will be lost in the ionosphere, and a loss cone will form for upward parallel velocity. This upward loss cone could contain electrons of ionospheric origin that have sufficient energy to overcome the parallel potential drop and escape, although generally the upward potential drop is much larger than the energy of the ionospheric electrons and so few electrons will populate this region. At large perpendicular velocity, we again have a population consisting of magnetospheric electrons that mirror before reaching the ionosphere. Near zero velocity is a region of electrons of ionospheric origin that do not have enough energy to overcome the parallel potential drop above the observation point. These electrons will be reflected by the electric field and returned to the ionosphere. These are referred to as backscattered electrons. Finally, there is the region between

the ellipse and the hyperbola. This region is not accessible to particles from either the ionospheric or magnetospheric sources. Any electron that enters this region is trapped by the magnetic mirror force below and the parallel electric field above the observation point. While it might be expected that this region would not have any particles, it is often observed that this region contains an enhancement in the distribution function. This indicates that the steady-state assumption on which this picture is based must break down.

A few features of these particle distributions should be made. First of all, it should be remembered that we assumed an upward parallel electric field. If the parallel electric field is in fact downward, then the roles of ions and electrons are exchanged, and Figure 1 would apply to electrons and Figure 2 to ions. Another important point to make regards the evolution of these features with altitude. As an electron beam moves down the field line, the loss cone angle  $\alpha$  increases. This would imply that a downgoing electron beam would spread out in pitch angle becoming more isotropic as it moves down the field line. Conversely, an upward going beam of ions (or electrons) will become more field aligned as it moves up the field line. Observations indicate that this is indeed the case. The primary downgoing electron beam, made up of magnetospheric electrons with a reasonably large perpendicular energy, spreads out in pitch angle at lower altitudes.

However, not all features of the auroral distribution can be simply described by this steady-state picture. One of the first non-adiabatic features observed in the auroral zone were the so-called ion conic distributions, which were first identified from S3-3 data by Sharp et al. (1977). Ion conics are distributions of ions of up to 20 keV energy whose distribution looks like a cone in velocity space with its symmetry axis along the upward  $v_{\parallel}$  axis. Ion conics are thought to be formed by the perpendicular heating of ions, presumably at the ion cyclotron frequency or its harmonics. These distributions are often observed to have a peak at an oblique angle, suggesting that their perpendicular heating is followed by acceleration up the field line due to the magnetic mirror force. Many wave modes have been suggested for this heating process (see, e.g., Lysak, 1986), which will be discussed in detail below. Upward going "electron conics" have also been observed (Menietti et al., 1985; Eliasson et al., 1996). Although superficially similar to the ion conics, the electron conics appear to be enhancements in the electron distribution that exist at the edge of the loss cone boundary. In addition, downgoing beams of electrons with very small pitch angles have been seen from sounding rockets (Johnstone and Winningham, 1982; McFadden et al., 1986) and more recently from the FAST satellite. The fact that these beams do not spread in pitch angle is evidence that they are formed from the parallel acceleration of cold beams of electrons. Such a particle distribution can not be easily formed from the purely static picture described here.

## 2. *Generalized Ohm's Law and Anomalous Resistivity*

The discussion in the previous session assumed that there was a field-aligned potential drop present on auroral field lines, and so the next task is to determine the physics behind the development of parallel electric fields in this region of space. This is an interesting question since according to the ideal, collisionless Ohm's Law,  $\mathbf{E} + \mathbf{v} \times \mathbf{B} / c = 0$ , which implies that the parallel electric field should be zero. Physically, this condition holds in a collisionless plasma since the light, essentially massless electrons are assumed to be able to short out any parallel electric fields by their rapid motion along the field line. As we saw in the first quarter of the

course, the Ohm's Law cited above is valid only as an approximation of the full "generalized" Ohm's Law, which is a consequence of the two-fluid picture of a plasma with only the assumption of a small mass ratio. This generalized Ohm's Law takes the form:

$$\mathbf{E} + \frac{\mathbf{v} \times \mathbf{B}}{c} = \eta \mathbf{j} + \frac{m_e}{ne^2} \left[ \frac{\partial \mathbf{j}}{\partial t} + \nabla \cdot \left( \mathbf{j} \mathbf{v} + \mathbf{v} \mathbf{j} - \frac{\mathbf{j} \mathbf{j}}{ne} \right) \right] + \frac{1}{nec} \mathbf{j} \times \mathbf{B} - \frac{1}{ne} \nabla \cdot \bar{\mathbf{P}}_e \quad (7)$$

(equation 3.33 from first quarter). If we take the parallel component of this equation by doing a dot product with a unit vector in the direction of the magnetic field, it can be written as:

$$E_{\parallel} = \eta j_{\parallel} + \frac{m_e}{ne^2} \frac{dj_{\parallel}}{dt} - \frac{1}{ne} (\nabla \cdot \bar{\mathbf{P}}_e)_{\parallel} \quad (8)$$

Here the total time derivative is meant to include all of the terms inside the bracket of equation (7). Thus, three effects can give rise to parallel electric fields in a two-fluid description of a plasma: resistivity, electron inertia, or electron pressure, corresponding respectively to the three terms on the RHS of equation (8).

In a collisionless plasma such as the auroral zone, particle-particle collisions do not give a significant resistivity, and so the first term is small unless wave-particle effects can give rise to an "anomalous resistivity." The other two terms can produce parallel electric fields in time-varying and nonuniform plasmas.

The most discussed candidate for anomalous resistivity has been the electrostatic ion cyclotron (EIC) wave, discussed by Kindel and Kennel (1971). These authors showed that the critical drift for the (EIC) instability was below that of the ion acoustic instability when the electron and ion temperatures were comparable. As we showed then, the critical drift for the EIC instability is  $v_d / a_i = 16.5$  for  $T_e = T_i$ .

It is worth emphasizing that, despite being called a "current-driven" instability, this instability, as well as the ion acoustic instability, is really driven by the relative drift between electrons and ions. This relative drift is given by  $v_d = j_{\parallel} / ne$ , and in general, both  $j_{\parallel}$  and  $n$  will vary along the field line. Consider a magnetic flux tube in which a field-aligned current flows. In general, in the collisionless magnetosphere, the steady-state perpendicular conductivity is zero, i.e., perpendicular currents cannot flow, aside from the effects of diamagnetic drifts or magnetic gradient-curvature drifts, both of which require the existence of hot plasma. Of course, perpendicular currents can also flow in the collisional ionosphere. In the topside ionosphere, however, collisions are unimportant, the plasma is relatively cold, and the curvature of the magnetic field is not strong, and so in the steady state, we expect all the current to flow along the magnetic field. (In a time-dependent situation, polarization currents which are proportional to the time derivative of the perpendicular electric field can also flow, which gives rise to Alfvén waves, which will be discussed shortly.)

If there are no perpendicular currents, current continuity demands that the total parallel current must be conserved. The current *density*, however, will change since the cross-section of the flux tube changes in a dipole field. Thus, if  $I_{\parallel}$  represents the total parallel current and  $A$  is the cross section of the flux tube, the current density is  $j_{\parallel} = I_{\parallel} / A$ . The cross section of the flux tube is defined by the requirement that the magnetic flux is constant, i.e.,  $\Phi_B = \int \mathbf{B} \cdot d\mathbf{A} \approx BA$ . Therefore, the current density can be written as  $j_{\parallel} = (I_{\parallel} / \Phi_B) B$ , and the drift velocity scales as  $v_d \propto B / n$ .

The implications of this scaling to the auroral zone were considered by Lysak and Hudson (1979). Using data from the S3-3 satellite (Mozer et al., 1979), in which the density

profile in the auroral zone was measured using the lower hybrid resonance frequency, we modeled the density by a function of the form:

$$n(\text{cm}^{-3}) = 1.34 \times 10^7 [h(\text{km})]^{-1.55} \quad (9)$$

where  $h$  is the altitude in kilometers. Using this profile, we found that the drift velocity for a given amount of current has a broad maximum at altitudes of 5000-8000 km. The drift velocity decreases at low altitudes due to the enhancement of the density as the ionosphere is approached, and it also decreases at high altitudes since the plasma density on auroral field lines becomes nearly constant while the magnetic field falls off roughly as  $r^{-3}$  due to the dipolar nature of the field.

It is worth noting that most theories of anomalous resistivity in the auroral zone are controversial, and no such theory has gained widespread acceptance in the auroral community. Thus, it is not clear what role if any that wave-particle interactions play in the formation of parallel electric fields. Nevertheless, the scaling of the drift velocity of the current as discussed above is relevant, as a number of other models for parallel electric fields are enhanced when the drift velocity is high.

### 3. Magnetic mirror effects on parallel electric fields

Of course, the fluid description of plasmas is an approximation to the kinetic theory of plasmas, and one might ask if the kinetic description can lead to parallel electric fields. A starting point for such a discussion is the electron and ion velocity space distributions discussed above. First of all, let us neglect any ion contribution to the field-aligned current density (observationally, the ion current is less than 10% of the electron current). Concentrating on the electrons, let us consider the upward current region where the parallel electric field is upward and the main electron motion is downward. If we assume that the magnetospheric source contains a bi-Maxwellian population (i.e., possibly different temperatures parallel and perpendicular to the magnetic field), then one can calculate the total flux of electrons that hit the ionosphere. The mirroring or trapped electrons do not contribute to the field-aligned current, since only electrons that move down the field line and do not go back up give a net current. Thus, the field-aligned current can be calculated by looking at the flux of electrons in the loss cone. Note that since the width of the loss cone increases as a function of the potential drop, the amount of current should also be a function of the potential. This procedure was first carried out by Knight (1973), and was discussed extensively by Fridman and Lemaire (1980). They found that the field-aligned current could be written as:

$$j_{\parallel} = -n_e e \sqrt{\frac{T_{\parallel}}{2\pi m_e}} \frac{B_I}{B_s} \left[ 1 - \frac{\exp(-xe\Delta\Phi/T_{\parallel})}{1+x} \right] \quad (10)$$

where  $n_e$ ,  $B_s$ ,  $T_{\parallel}$  and  $T_{\perp}$  are the density, magnetic field, and parallel and perpendicular temperatures in the source,  $B_I$  is the magnetic field at the ionosphere,  $\Delta\Phi$  is the potential drop and the quantity  $x = (T_{\parallel}/T_{\perp})/(B_I/B_s - 1)$ . The factors outside the brackets simply give the thermal current along the field line in the source, multiplied by the magnetic field ratio that takes into account the fact that the current flows along a flux tube that becomes smaller as the magnetic field becomes larger. The factor in the brackets gives the fraction of the downgoing electrons that are in the loss cone. Note that this factor becomes one when the potential drop is

very large, indicating that all downgoing electrons are lost into the ionosphere.

If we note that  $B_l \gg B_s$  if the source is far out in the magnetosphere, the quantity  $x$  is generally much less than one. If we have  $xe\Delta\Phi/T_{\parallel} \ll 1$ , we can expand the exponential to first order in the potential drop, which gives:

$$j_{\parallel} = -n_e e \sqrt{\frac{T_{\parallel}}{2\pi m_e} \frac{B_l}{B_s} \frac{x}{1+x}} \left( 1 + \frac{e\Delta\Phi}{T_{\parallel}} \right) \quad (11)$$

If  $e\Delta\Phi/T_{\parallel} \gg 1$ , equation (11) can be written as a linear current-voltage relation  $j_{\parallel} = -K \Delta\Phi$ , where the coefficient  $K$  has the form:

$$K = \frac{n_e e^2}{T_{\perp} (1 - B_s/B_l)} \sqrt{\frac{T_{\parallel}}{2\pi m_e}} \quad (12)$$

If we consider currents flowing on auroral field lines, typical numbers would give  $T_{\parallel} \sim T_{\perp} \sim 100$  eV and  $B_l/B_s \sim 1000$ , then  $x \sim 10^{-3}$ . For these parameters, the linear current-voltage relation is valid for potential drops between 100 eV and 100 keV, which encompasses a great deal of the region of interest for auroral particles. Thus, this linear current-voltage relation is often used in auroral ionosphere. For these parameters and a density of  $1 \text{ cm}^{-3}$ , the constant  $K \sim 10^{-9} \text{ mho/m}^2$ . Note that this value gives a current of  $1 \mu\text{A/m}^2$  for a voltage drop of 1 kV.

On the other hand, some authors have taken this relationship, sometimes referred to as the Knight relation, to describe the cause of parallel electric fields in the auroral zone. This view is mistaken (in the opinion of the author of these notes), since equation (10) only describes the response of the auroral particles to an imposed potential drop. To describe the causes of parallel electric fields in a model such as this requires additional information; in particular, one must ensure that the parallel electric field is consistent with Poisson's equation or, more simply, a quasi-neutrality condition. An early model of this type was introduced by Alfvén and Fälthammar (1963), who considered a simple model consisting of monoenergetic population of electrons and ions that had both parallel and perpendicular energies. Their idea was that if the electrons and ions had different pitch angles, they would mirror at different altitudes producing a charge imbalance. This leads to a parallel electric field being set up that would adjust the electron and ion distributions so that quasi-neutrality was maintained at all locations along the field line. They found a parallel electric field given by:

$$E_{\parallel} = -\frac{W_{\parallel} W_{e\perp} - W_{e\parallel} W_{i\perp}}{e B_s (W_{e\parallel} + W_{i\parallel})} \frac{dB}{ds} \quad (13)$$

where the  $W$  terms are the electron and ion energies parallel and perpendicular to the field in the source region, and  $s$  is the distance along the field line. Note that the parallel electric field goes to zero if the electrons and ions have the same pitch angle, i.e.,  $W_{e\perp}/W_{e\parallel} = W_{i\perp}/W_{i\parallel}$ . An upward parallel electric field is produced if the electrons are more perpendicular than the ions, and vice versa.

This model faces the difficulty that it must be very tightly tuned in order to give reasonable potential drops. Integrating (13) along the field line gives a potential drop  $\Delta\Phi = (\delta W/e)(B_l/B_s - 1)$ , where  $\delta W$  represents the energy factors in (13). Since  $B_l \gg B_s$ , the energy factor  $\delta W$  must only be a few eV despite the fact that the individual energy terms should be the order of 1 keV. Thus, this model would require a high degree of fine tuning to consistently produce potential drops in the 1-10 kV range that is observed. Of course, the model

is highly idealized: in practice, there is a range of energies in the electron and ion distributions, and in addition, quasi-neutrality can be maintained by the addition of ionospheric particles. A numerical model that contained more realistic populations was developed by Chiu and Schulz (1978) and Chiu and Cornwall (1980). These studies differ in that the former assumed quasi-neutrality while the latter solved the full Poisson equation. These authors iterated the particle populations and the parallel potential drop in an attempt to converge toward a solution. They found parallel electric field distributions that, in agreement with equation (13), scaled with the magnetic field gradient, but had a more reasonable value of the total potential drop. A difficulty with this model is that they needed to assume a rather high lower boundary condition (2000 km), below which the plasma was assumed to become collisional. This was a bit troublesome since the maximum parallel electric field then occurred right above the lower boundary where the magnetic field gradient is the strongest. Perhaps most importantly, this model was intrinsically steady state and difficult to generalize to a time-dependent situation. Thus, while models of this sort might account for the structure of a steady aurora arc, they fail in time-dependent situations such as active auroral forms. It is important to note, however, that the Knight relation (10) is not affected by the drawbacks in this theory, and should apply to adiabatically moving particles in any potential gradient.

A more sophisticated model of this sort has recently been presented by Ergun et al. (2000). In this model, they included 8 different particle populations: Ionosphere hydrogen and oxygen ions, magnetospheric hydrogen, cold ionospheric electrons, primary magnetospheric electrons, backscattered primary electrons, secondary electrons (ionospheric electrons that are energized by collisions with the primaries), and electrons in the trapped region (cf. Figure 2). They found that one or two strong “transition layers” containing large parallel potential drops occurred in localized regions along the auroral field line. Such regions may be described by the BGK double layer theory discussed in the next section.

### 3. Plasma double layers.

The so-called plasma double layer is an example of a nonlinear wave that can be treated by the BGK theory, in which electrostatic nonlinear wave structures are formed self-consistently with the particle populations that provide the charge density that supports the wave. The plasma double layer is a stationary potential structure consisting of a potential step. These structures have been extensively studied since such a potential step would be an efficient accelerator of particles. It is thought by some that such a structure, or perhaps a series of such structures, may be responsible for the particle acceleration in the auroral zone. The name is due to the fact that such a potential structure can be maintained by two layers of charge, one positive and one negative. This can be seen from this figure by noting that the charge is the second derivative of the potential, and thus the upward curving part of the potential for  $x < 0$  is associated with a negative charge layer and the region of downward curvature for  $x > 0$  corresponds to a positive charge layer. The full phase space structure for both electrons and ions is shown in Figure 3. Note that the electron potential energy takes a downward step with increasing  $x$ , and so the electron phase space is a mirror reflection of the ion phase space diagram.

We may determine the qualitative form of the Sagdeev potential for this problem from noting the potential step structure. The Sagdeev potential must have maxima both at the origin and at the point  $\Phi = \Phi_0$ , where  $\Phi_0$  is the amplitude of the double layer, as is shown in Figure 3. If we note that the Sagdeev potential is related to the double layer by the relation:

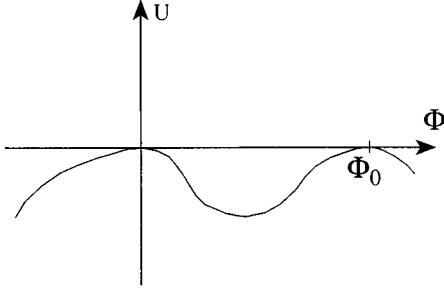


**Fig. 3. Sketch of the Sagdeev potential for a double layer.**

derivative of the Sagdeev potential is negative at both boundaries, which implies that the first derivative of the charge density is negative. Thus, as stated previously, the charge density must be negative near  $\Phi=0$  and positive as  $\Phi$  approaches  $\Phi_0$ .

Thus, let us see what types of particle populations we would need to have to support such a double layer. Since the importance of these double layers is to accelerate particles, it would seem that a minimal set of populations would be a cold ion beam entering from the right hand side of Figure 7.8, and a cold electron beam entering from the left hand side. Let us see if these two populations are sufficient to support the double layer. First, consider an ion beam with a density  $n_{i0}$  and a velocity  $u_{i0}$  at  $x=+\infty$  where the potential is  $\Phi_0$ . At any other position  $x$  energy conservation gives:

$$\frac{1}{2}Mu_i^2 + e\Phi = \frac{1}{2}Mu_{i0}^2 + e\Phi_0 \quad (16)$$

where  $u_i$  and  $\Phi$  are the values at the point  $x$ . Using this relation and the continuity equation, the ion density is given by:

$$n_i = \frac{n_{i0}u_{i0}}{u_i} = \frac{n_{i0}}{\sqrt{1 + 2e(\Phi_0 - \Phi)/Mu_{i0}^2}} \quad (17)$$

For the electrons, we can let define the density  $n_{e0}$  and  $u_{e0}$  at  $x=-\infty$  where  $\Phi = \Phi_0$ . Then the electron energy equation is:

$$\frac{1}{2}mu_e^2 - e\Phi = \frac{1}{2}mu_{e0}^2 \quad (18)$$

and the density will be:

$$n_e = \frac{n_{e0}u_{e0}}{u_e} = \frac{n_{e0}}{\sqrt{1 + 2e\Phi/mu_{e0}^2}} \quad (19)$$

As noted above, the charge density must be zero, i.e., the electron and ion densities must be equal, at the boundaries where  $\Phi = 0$  and  $\Phi = \Phi_0$ . These two conditions require:

$$n_{e0} = \frac{n_{i0}}{\sqrt{1 + 2e\Phi_0/Mu_{i0}^2}} \quad (20)$$

and:

$$n_{i0} = \frac{n_{e0}}{\sqrt{1 + 2e\Phi_0/mu_{e0}^2}} \quad (21)$$

It can be easily seen that these two conditions are incompatible with each other. Physically, this

$$\Phi'' = -\frac{dU}{d\Phi} = -\frac{\rho}{\epsilon_0} \quad (14)$$

we can see that the Sagdeev potential is given by:

$$U(\Phi) = \frac{1}{\epsilon_0} \int_0^\Phi \rho(\Phi') d\Phi' \quad (15)$$

Then we can note a few properties of this solution. First of all, since the Sagdeev potential is zero at  $\Phi=0$  and  $\Phi=\Phi_0$ , we note that the total charge in the system must vanish. In addition, the derivative of the Sagdeev potential is 0 at these two end points, thus, the charge density is zero at the boundaries. Finally, the second

results from the fact that an accelerated beam decreases in density, and so the ion density is smaller on the left while the electron density is smaller on the right.

Thus, in order to support this solution, we need to add electrons on the right and ions on the left, which can be done by adding a reflected population of ions and electrons. If we assume that these reflected populations are described by a Boltzmann factor, the total densities of the two species can be written as:

$$n_i = \frac{n_{i0}}{\sqrt{1 + 2e(\Phi_0 - \Phi)/Mu_{i0}^2}} + n_{it}e^{-e\Phi/T_i} \quad (22)$$

and

$$n_e = \frac{n_{e0}}{\sqrt{1 + 2e\Phi/mu_{e0}^2}} + n_{et}e^{e(\Phi - \Phi_0)/T_e} \quad (23)$$

where  $n_{it}$  is the trapped ion density at  $\Phi = 0$  and  $n_{et}$  is the trapped electron density at  $\Phi = \Phi_0$ . We now clearly have enough parameters to insure quasi-neutrality at the two boundaries.

Let us now calculate the contributions to the Sagdeev potential for each of these for populations by using (15). The ion beam contribution is given by:

$$\begin{aligned} U_{ib}(\Phi) &= \frac{n_{i0}e}{\epsilon_0} \int_0^\Phi \frac{d\Phi'}{\sqrt{1 + 2e(\Phi_0 - \Phi)/Mu_{i0}^2}} \\ &= \frac{n_{i0}Mu_{i0}^2}{\epsilon_0} \left[ \sqrt{1 + \frac{2e\Phi_0}{Mu_{i0}^2}} - \sqrt{1 + \frac{2e(\Phi_0 - \Phi)}{Mu_{i0}^2}} \right] \end{aligned} \quad (24)$$

and the electron beam contribution can be evaluated similarly:

$$U_{eb}(\Phi) = -\frac{n_{e0}mu_{e0}^2}{\epsilon_0} \left[ \sqrt{1 + \frac{2e\Phi}{mu_{e0}^2}} - 1 \right] \quad (25)$$

The trapped ion population contribution is:

$$\begin{aligned} U_{it}(\Phi) &= \frac{n_{it}e}{\epsilon_0} \int_0^\Phi e^{-e\Phi'/T_i} d\Phi' \\ &= \frac{n_{it}T_i}{\epsilon_0} (1 - e^{-e\Phi/T_i}) \end{aligned} \quad (26)$$

and the trapped electrons give:

$$U_{et}(\Phi) = -\frac{n_{et}T_e}{\epsilon_0} \left[ e^{e(\Phi - \Phi_0)/T_e} - e^{-e\Phi_0/T_e} \right] \quad (27)$$

Putting all of these together gives:

$$\begin{aligned} U(\Phi) &= \frac{1}{\epsilon_0} \left[ n_{i0}Mu_{i0}^2 \left[ \sqrt{1 + \frac{2e\Phi_0}{Mu_{i0}^2}} - \sqrt{1 + \frac{2e(\Phi_0 - \Phi)}{Mu_{i0}^2}} \right] - n_{e0}mu_{e0}^2 \left( \sqrt{1 + \frac{2e\Phi}{mu_{e0}^2}} - 1 \right) \right. \\ &\quad \left. + n_{it}T_i (1 - e^{-e\Phi/T_i}) - n_{et}T_e (e^{e(\Phi - \Phi_0)/T_e} - e^{-e\Phi_0/T_e}) \right] \end{aligned} \quad (28)$$

Note that  $U(0)$  is equal to zero by construction; therefore, the quasi-neutrality condition at  $\Phi = \Phi_0$  is equivalent to saying  $U(\Phi_0) = 0$ . This condition can be written:

$$0 = U(\Phi_0) = \frac{1}{\epsilon_0} \left[ n_{i0} M u_{i0}^2 \left[ \sqrt{1 + \frac{2e\Phi_0}{M u_{i0}^2}} - 1 \right] - n_{e0} m u_{e0}^2 \left( \sqrt{1 + \frac{2e\Phi_0}{m u_{e0}^2}} - 1 \right) + n_{it} T_i (1 - e^{-e\Phi_0/T_i}) - n_{et} T_e (1 - e^{-e\Phi_0/T_e}) \right] \quad (29)$$

It would clearly be difficult to make much sense out of the condition (29) in the general case, so we will restrict this discussion to the *strong double layer limit*, which states that the potential energy change across the double layer is much larger than any other energy in the system, i.e.,  $e\Phi_0 \gg M u_{i0}^2, m u_{e0}^2, T_i, T_e$ . Then, the quasi-neutrality condition gives:

$$U(\Phi_0) = \frac{1}{\epsilon_0} \left[ n_{i0} u_{i0} \sqrt{2Me\Phi_0} - n_{e0} u_{e0} \sqrt{2me\Phi_0} + n_{it} T_i - n_{et} T_e \right] = 0 \quad (30)$$

This condition can be rewritten:

$$n_{e0} u_{e0} = n_{i0} u_{i0} \sqrt{\frac{M}{m}} + \frac{n_{it} T_i - n_{et} T_e}{\sqrt{2me\Phi_0}} \approx n_{i0} u_{i0} \sqrt{\frac{M}{m}} \quad (31)$$

where the last inequality follows from the strong double layer limit. This equation is known as the *Langmuir condition*, and it states that the electron flux is much greater than the ion flux through the double layer, or equivalently that the electrons carry most of the current through the double layer.

It is somewhat curious that although we cannot make a double layer without the trapped particles, information about the trapped particles disappears from the Langmuir condition in the strong double layer limit. Nevertheless, the trapped particles are essential to the structure. (Actually it can be shown that only one of the trapped populations is necessary.) We do, however, have an additional condition to fill, namely that the Sagdeev potential be a local maximum at  $\Phi = 0$  and at  $\Phi_0$ . The second derivative of (28) yields:

$$U''(\Phi) = \frac{e^2}{\epsilon_0} \left[ \frac{n_{i0}}{M u_{i0}^2} \left( 1 + \frac{2e(\Phi_0 - \Phi)}{M u_{i0}^2} \right)^{-3/2} + \frac{n_{e0}}{m u_{e0}^2} \left( 1 + \frac{2e\Phi}{m u_{e0}^2} \right)^{-3/2} - \frac{n_{it}}{T_i} e^{-e\Phi/T_i} - \frac{n_{et}}{T_e} e^{e(\Phi - \Phi_0)/T_e} \right] \quad (32)$$

It can be seen that the beam terms in this expression give only positive contributions to the second derivative; thus, the trapped particles are essential to make the second derivative negative at the boundaries. Evaluating (32) at  $\Phi = \Phi_0$  and applying the strong double layer approximation gives:

$$\frac{\epsilon_0}{e^2} U''(\Phi_0) \approx \frac{n_{i0}}{M u_{i0}^2} + \frac{n_{e0} u_{e0} \sqrt{m}}{(2e\Phi_0)^{3/2}} - \frac{n_{et}}{T_e} < 0 \quad (33)$$

Applying the Langmuir condition  $n_{e0} u_{e0} \sqrt{m} = n_{i0} u_{i0} \sqrt{M}$ , we can write this condition as:

$$\frac{n_{i0}}{M u_{i0}^2} \left( 1 + \frac{1}{2} \left( \frac{M u_{i0}^2}{e\Phi_0} \right)^{3/2} \right) < \frac{n_{et}}{T_e} \quad (34)$$

Finally, we may note that quasi-neutrality at  $\Phi = \Phi_0$  requires that:

$$n_{et} = n_{i0} - n_{e0} u_{e0} \sqrt{\frac{m}{2e\Phi_0}} = n_{i0} \left( 1 - \sqrt{\frac{Mu_{i0}^2}{2e\Phi_0}} \right) \approx n_{i0} \quad (35)$$

Thus, combining (34) and (35), and ignoring terms of order  $\sqrt{Mu_{i0}^2/2e\Phi_0}$ , we find a simple condition, known as the *Bohm criterion*:

$$u_{i0}^2 > \frac{T_e}{M} \quad (36)$$

This condition implies that the ion beam must flow into the double layer at a speed exceeding the ion acoustic speed. Recalling that the ion velocity is essentially the center-of-mass velocity for the system, this condition can also be interpreted to say that the double layer propagates through the plasma with a speed greater than the ion acoustic speed. It should be noted that similar considerations at  $\Phi=0$  lead to the condition  $u_{e0}^2 > T_i/m$ . If the initial beam densities for the electrons and ions are equal and the temperatures of the trapped particles are as well, these two conditions are equivalent.

The above considerations are an example of how the BGK theory can be used in conjunction with physically reasonable assumptions to establish conditions for the existence of a nonlinear wave in a plasma. As a practical matter, this type of calculation is restricted to one-dimensional, unmagnetized situations, yet it is still of some use in describing these nonlinear waves. The physics that is missing in such calculations is any information on the evolution of these nonlinear structures, in particular, the mechanism by which such a quasi-steady wave may be established in the first place. Such structures may arise from a turbulent situation by some sort of self-organization process, but the description of the details of this evolution is still an open question. We will discuss some aspects of the nonlinear evolution of waves in the next chapter, but it should be emphasized that many aspects of this question remain unanswered.

#### 4. *The thickness of auroral arcs: the role of the ionosphere*

Perhaps the most striking feature of observed auroral arcs is their narrow width in one direction perpendicular to the magnetic field. By making observations in the magnetic zenith, where projection effects do not obscure the true thickness of the observed aurora, Maggs and Davis (1968) showed that individual auroral arcs could have thicknesses down to 100 m. These observations were repeated and confirmed by Borovsky and Suszcynsky (1993). More recently, arcs at an even narrower scale size were reported at the IAGA meeting in Uppsala (1997) by T. S. Trondsen. These narrow scale sizes are in contrast with early observations of auroral particles that indicated that electron precipitation structures in the auroral zone had a thickness of a few to a few tens of kilometers (e.g., Arnoldy, 1977; Evans et al., 1977). Borovsky (1993a) has pointed out that no theory of auroral arcs has yet produced a satisfactory picture of such a wide range of scales. Thus, it is a major challenge to auroral theory to account for auroral arcs on scales of tens of meters to tens of kilometers.

The simplest model of auroral arc scales comes from the electrostatic theory including the Knight relation (11) in its linearized form,  $j_{\parallel} = -K(\Phi_I - \Phi_s)$ , where we explicitly write out the ionospheric and source potentials. Note that in this relation, upward field-aligned current is negative, since in the northern hemisphere the magnetic field direction is downward. In order to derive a scale size from this relationship, we need to consider the closure of this field-aligned current in the ionosphere. The field-aligned current closes in the ionosphere by means of

perpendicular currents that flow due to the finite Hall and Pedersen conductivities. The Ohm's Law for perpendicular currents can be written in the form:

$$\mathbf{j}_\perp = \begin{pmatrix} \sigma_P & -\sigma_H \\ \sigma_H & \sigma_P \end{pmatrix} \cdot \mathbf{E}_\perp \quad (37)$$

where the Pedersen and Hall conductivities are given by (e.g., Kelley, 1989):

$$\sigma_P = \sum_s \frac{n_s q_s^2}{m_s} \frac{v_s}{v_s^2 + \Omega_s^2} \quad \sigma_H = -\sum_s \frac{n_s q_s^2}{m_s} \frac{\Omega_s}{v_s^2 + \Omega_s^2} \quad (38)$$

where  $v_s$  is the collision frequency of species  $s$  and the gyrofrequency  $\Omega_s$  contains the sign of the charge (i.e., is negative for electrons). Physically, the Pedersen conductivity occurs when the ion collision frequency is approximately equal to the gyrofrequency, allowing the ions to move in the direction of the applied electric field, while the Hall conductivity is greatest when the ions are strongly tied to the neutral atmosphere by collisions while the electrons are free to execute an  $\mathbf{E} \times \mathbf{B}$  drift. Note that we can also write (37) in the vector form:

$$\mathbf{j}_\perp = \sigma_P \mathbf{E}_\perp - \sigma_H \mathbf{E}_\perp \times \hat{\mathbf{b}} \quad (39)$$

where  $\hat{\mathbf{b}}$  is the unit vector in the magnetic field direction.

Current continuity and the absence of any charge build-up in the ionosphere indicate that the total current must be divergence-free, i.e.,  $\nabla \cdot \mathbf{j} = 0$ . If we assume for a moment that the magnetic field lines are exactly vertical, and that the  $z$  direction points vertically downward, then the current continuity condition can be written as:

$$\nabla_\perp \cdot \mathbf{j}_\perp = -\frac{\partial j_\parallel}{\partial z} \quad (40)$$

Now we can take advantage of the fact that the ionosphere can be considered to be a thin slab, since the current carrying region of the ionosphere has a scale of about 150 km. We can then integrate equation (40) over the height of the ionosphere, yielding:

$$\nabla_\perp \cdot \mathbf{I}_\perp = -(j_\parallel^{\text{bottom}} - j_\parallel^{\text{top}}) = j_\parallel^{\text{top}} \quad (41)$$

where *top* and *bottom* refer to the field-aligned current through the top and bottom surfaces of the ionosphere, and  $\mathbf{I}_\perp = \int dz \mathbf{j}_\perp$  is the perpendicular current integrated over the ionosphere. The last step in (41) follows by the assumption that no current flows out the bottom of the ionosphere into the atmosphere.

Note that if the magnetic field is not strictly vertical, the current entering the ionosphere is reduced by the sine of the inclination angle, and so (132) should be written as  $\nabla_\perp \cdot \mathbf{I}_\perp = j_\parallel \sin i$ , where  $i$  is the inclination angle ( $90^\circ$  for a vertical field). For a dipole field, the magnetic field can be written as:

$$\mathbf{B} = -\frac{B_0 R_E^3}{r^3} (\hat{\mathbf{r}} 2 \cos \theta + \hat{\boldsymbol{\theta}} \sin \theta) \quad (42)$$

where  $\theta$  is the co-latitude. Thus, the inclination angle is given by  $\tan i = B_r / B_\theta = 2 \cot \theta$ . The auroral zone is roughly at a latitude of  $70^\circ$ , or a co-latitude of  $20^\circ$ . Thus, the inclination angle is about  $80^\circ$  whose sine is 0.983. Thus, neglecting the inclination angle is a reasonably good approximation (to within 2%) in the auroral zone, and we will make this approximation in what follows.

The height-integrated current in equation (41) can be written in terms of a height-

integrated conductivity tensor,  $\bar{\Sigma} = \int dz \bar{\sigma}$ . Inserting these quantities into equation (39) and additionally assuming that the electric field in the ionosphere is electrostatic,  $\mathbf{E}_\perp = -\nabla_\perp \Phi_I$ . Then we can write equation (41) as:

$$j_{\parallel} = -\Sigma_p \nabla_\perp^2 \Phi_I - \nabla_\perp \Sigma_p \cdot \nabla_\perp \Phi_I + (\nabla_\perp \Sigma_H \times \nabla_\perp \Phi_I) \cdot \hat{\mathbf{b}} \quad (43)$$

Note that if the conductivities are uniform, only the first term on the RHS of (43) survives. In this case, we can use (43) together with the Knight relation to eliminate the field-aligned current, and write:

$$\Sigma_p \nabla_\perp^2 \Phi_I = K (\Phi_I - \Phi_s) \quad (44)$$

or:

$$\left(1 - \frac{\Sigma_p}{K} \nabla_\perp^2\right) \Phi_I = \Phi_s \quad (45)$$

Equation (45) then gives the ionospheric potential in response to an imposed potential in the source region. It is important to note that this equation contains a new scale length  $\lambda_{MI} = \sqrt{\Sigma_p / K}$ , which is sometimes termed the magnetosphere-ionosphere coupling scale length. For typical values of  $\Sigma_p = 10$  mho and  $K = 10^{-9}$  mho/m<sup>2</sup>, this scale length is 100 km.

The physical significance behind this expression can be seen if we Fourier analyze the fields in the perpendicular direction. Then the ionospheric potential becomes:

$$\Phi_I = \frac{\Phi_s}{1 + k^2 \lambda_{MI}^2} \quad (46)$$

and the parallel potential drop can be written as:

$$\Delta\Phi = \Phi_I - \Phi_s = -\Phi_s \frac{k^2 \lambda_{MI}^2}{1 + k^2 \lambda_{MI}^2} \quad (47)$$

Thus, the parallel potential drop is small for large-scale structures  $k\lambda_{MI} \ll 1$ , and can approach the full value of the source potential for small structures. Therefore  $\lambda_{MI}$  represents a maximum scale size for auroral potential drops. Note also that because of the minus sign in (47), a negative potential in the source is necessary for a positive potential drop, i.e., one that leads to an upward parallel electric field and field-aligned current. Thus, the field-aligned current can be roughly considered to be the response of the plasma to a negative space charge in the outer magnetosphere that repels electrons down the field line to create the upward field-aligned current.

Note that the MI coupling scale length is quite large and so cannot explain the scale size of individual auroral arcs. It does, however, give an indication of the largest potential structures that could be formed, and indeed, auroral structures are rarely seen on scales greater than 100 km. Further investigations of the implications of this type of model can be found in Lyons (1980) and Lysak (1985).

## B. Time-dependent magnetosphere-ionosphere coupling: kinetic Alfvén waves

The considerations discussed previously have all been based on a steady-state picture of magnetosphere-ionosphere coupling. While steady auroral arcs are commonly observed, it is perhaps more typical for the aurora to be very dynamic, constantly moving and changing in brightness. Thus, it seems clear that a time-dependent model of auroral currents should be

considered. Since the changes in the aurora should be associated with changes in the field-aligned current, the dynamics of such current changes is important. Within the context of MHD theory, the wave that carries field-aligned current is the intermediate or shear Alfvén wave. As it turns out, when the perpendicular wavelength of these Alfvén waves becomes small, the ideal MHD description of the plasma breaks down. This breakdown can be described in terms of the generalized Ohm's Law, equation (7), or more fundamentally, in terms of kinetic theory. In this section, we will first consider the fluid description of shear Alfvén waves, both from an ideal MHD point of view and from a two-fluid model. We will then discuss the fully kinetic dispersion relation.

### 1. Ideal MHD model of shear Alfvén waves and their reflection from the ionosphere

Of the three MHD wave modes, only the shear Alfvén wave carries a field-aligned current. This wave is magnetically incompressible, meaning that the wave changes the direction but not the magnitude of the magnetic field strength. Thus, the simplest model for this wave involves the ideal, incompressible MHD equations. If we assume that the background magnetic field  $\mathbf{B}_0$  is directed along the  $z$  direction, these equations can be written in terms of the velocity perturbation  $\mathbf{v}$  and the magnetic perturbation, which we will denote by a lower case vector  $\mathbf{b}$ . Then the relevant linearized equations become:

$$\rho \frac{\partial \mathbf{v}}{\partial t} = \frac{\mathbf{j} \times \mathbf{B}_0}{c} = \frac{1}{4\pi} \mathbf{B}_0 \cdot \nabla \mathbf{b} \quad (48)$$

$$\frac{\partial \mathbf{b}}{\partial t} = \nabla \times (\mathbf{v} \times \mathbf{B}_0) = \mathbf{B}_0 \cdot \nabla \mathbf{v} \quad (49)$$

Note that these equations have been simplified by assuming that the background magnetic field is uniform, and by making the incompressible assumptions that  $\mathbf{B}_0 \cdot \mathbf{b} = 0$  and  $\nabla \cdot \mathbf{v} = 0$ . Fourier transforming these equations in the usual manner leads to the dispersion relation  $\omega = k_{\parallel} V_A$  where the Alfvén speed is defined by  $V_A = B_0 / \sqrt{4\pi\rho}$ . Note as well that the velocity and magnetic field perturbations are related in a similar manner as  $\mathbf{v} = \mp \mathbf{b} / \sqrt{4\pi\rho}$ , where the top sign (negative) applies for propagation parallel and the bottom sign (positive) for propagation anti-parallel to  $\mathbf{B}_0$ .

To look at the wave properties, note first that the electric field is given by the ideal Ohm's Law:

$$\mathbf{E}_{\perp} = -\frac{\mathbf{v} \times \mathbf{B}_0}{c} = \pm \frac{\mathbf{b} \times \mathbf{B}_0}{c\sqrt{4\pi\rho}} = \pm \frac{V_A}{c} \mathbf{b} \times \hat{\mathbf{z}} \quad (50)$$

Thus, it can be seen that the ratio of the electric field to the magnetic perturbation is just  $V_A / c$ , and that the electric field is perpendicular to the magnetic field perturbation. Note also that the perpendicular current can be calculated from Ampere's Law:

$$\mathbf{j}_{\perp} = \frac{c}{4\pi} \nabla \times \mathbf{b} = \frac{c}{4\pi} \frac{\partial}{\partial z} (\hat{\mathbf{z}} \times \mathbf{b}) \quad (51)$$

Assuming the magnetic field is then uniform, we can write a relation between the current and the electric field:

$$\mathbf{j}_{\perp} = \mp \frac{c^2}{4\pi V_A} \frac{\partial \mathbf{E}_{\perp}}{\partial z} \quad (52)$$

The coefficient in this expression can be written in terms of an effective conductance known as

the Alfvén conductance,  $\Sigma_A = c^2 / 4\pi V_A$ .

If we then consider the parallel component of the current, Ampere's Law implies that:

$$j_{\parallel} = \frac{c}{4\pi} (\nabla \times \mathbf{b})_{\parallel} = \frac{c}{4\pi} \left( \frac{\partial b_y}{\partial x} - \frac{\partial b_x}{\partial y} \right) \quad (53)$$

Note that unlike any of the wave properties listed before, the field-aligned current depends on the perpendicular wavelength of the wave. Thus, in the limit of infinite perpendicular wavelength, there is no field-aligned current; however, in any real system, there must be a finite size to the wave in the perpendicular direction, and so the field-aligned current is non-zero.

Let us consider what happens when the Alfvén wave is incident on the ionosphere. If the conductivity is uniform, then the field-aligned current is related to the perpendicular electric field in the ionosphere by equation (43), which can be written in this case as:

$$j_{\parallel} = \Sigma_P \nabla_{\perp} \cdot \mathbf{E}_{\perp} \quad (54)$$

Using equation (50), we can write  $\mathbf{b} = \pm(c/V_A)\hat{\mathbf{z}} \times \mathbf{E}_{\perp}$ , and inserting this into (53), we can write the field-aligned current in the wave as:

$$j_{\parallel} = \pm \frac{c^2}{4\pi V_A} \nabla_{\perp} \times (\hat{\mathbf{z}} \times \mathbf{E}_{\perp}) = \pm \Sigma_A \nabla_{\perp} \cdot \mathbf{E}_{\perp} \quad (55)$$

Now, consider the northern hemisphere situation where the background magnetic field is into the ionosphere. Then, the incident (downgoing) Alfvén wave will have the plus sign in (55), while the reflected (upgoing) wave will have the minus sign. Writing both sides of (54) in terms of a sum of the two waves, we have:

$$j_{\parallel}^{inc} + j_{\parallel}^{ref} = \Sigma_A \nabla_{\perp} \cdot (\mathbf{E}_{\perp}^{inc} - \mathbf{E}_{\perp}^{ref}) = \Sigma_P \nabla_{\perp} \cdot (\mathbf{E}_{\perp}^{inc} + \mathbf{E}_{\perp}^{ref}) \quad (56)$$

which can be written as:

$$\nabla_{\perp} \cdot [(\Sigma_A - \Sigma_P)\mathbf{E}_{\perp}^{inc} - (\Sigma_A + \Sigma_P)\mathbf{E}_{\perp}^{ref}] = 0 \quad (57)$$

Assuming a localized wave with fields that go to zero at some boundary, we can integrate (57) and write it in terms of a reflection coefficient for the electric field:

$$R \equiv \frac{E_x^{ref}}{E_x^{inc}} = \frac{\Sigma_A - \Sigma_P}{\Sigma_A + \Sigma_P} \quad (58)$$

This reflection coefficient was first derived by Scholer (1970) and was extensively used by Mallinckrodt and Carlson (1978) in their modeling of Alfvén wave interactions with the ionosphere.

Equation (58) is rich in consequences. First of all, it can be seen that the reflection is not present if the Pedersen and Alfvén conductivities are equal. This has a direct analogy with the termination of a transmission line by a resistor: if the impedances match, there is no reflection. In general, however, these conductivities are not matched. The most typical case is that the Pedersen conductivity, which is generally 1-10 mho in the ionosphere, is larger than the Alfvén conductivity, which is usually less than 0.5 mho (Lysak and Hudson, 1987; Lysak, 1990). It is easy to see that in this case, the reflection coefficient is negative, implying that the electric field in the reflected wave is in the opposite direction as the electric field in the incident wave. Thus if these two waves are superimposed, the net effect is to reduce the electric field strength. Indeed, in the extreme limit of infinite ionospheric conductivity ( $\Sigma_P \gg \Sigma_A$ ), the reflection coefficient is  $-1$  and the reflected electric field cancels the incident field. In this case the ionosphere can be said to short out the perpendicular electric field.

On the other hand, the reflected wave magnetic field has a relative minus sign with respect to the incident field, and so if the reflected electric field is in the opposite direction as the incident field, i.e.,  $R < 0$ , the reflected magnetic field reinforces the incident wave magnetic field. Thus the high conductivity ionosphere tends to enhance the perpendicular magnetic field and thus the field-aligned current. Of course the opposite conclusions can be drawn in the case when  $\Sigma_P < \Sigma_A$ , such as could happen at night or in the winter in the absence of any particle precipitation, when the conductivity can be as low as 0.1 mho. This type of highly resisting ionosphere tends to restrict the flow of current and enhance the electric field.

When there is a mismatch between the conductivities, it is difficult for an Alfvén wave to quickly establish a steady-state current system. If one were to arbitrarily launch an Alfvén wave from the magnetosphere and allow it to propagate to the ionosphere, the wave would begin bouncing back and forth. Suppose a fixed electric field were imposed at the magnetospheric end of a flux tube in a generator region (Lysak and Dum, 1983). This electric field would propagate to the ionosphere as an Alfvén wave, and reflection would occur according to the reflection coefficient (58), reducing the electric field (assuming  $\Sigma_P > \Sigma_A$ ) and increasing the field-aligned current. The reflected wave propagates back to the generator, in which the perpendicular electric field is fixed, and another Alfvén wave is launched back toward the ionosphere. Each time the wave interacts with the ionosphere, the net result is that the ionospheric electric field is increased by a relative amount equal to  $1 - |R|$ . Thus if  $R$  is very close to  $-1$ , a great number of bounces are needed to impose an electric field on the ionosphere, while if  $R$  is nearly zero, fewer bounces are required. A similar scenario is found if a fixed magnetic perturbation is imposed at the generator, although in this case the electric field and field-aligned current overshoot their initial values and approaches a steady state in an oscillatory manner (Lysak and Dum, 1983). A detailed study of the differences between these voltage and current generators is found in Lysak (1985).

The reflection of Alfvén waves is modified if a parallel electric field occurs along auroral field lines. In this case, the ionospheric and magnetospheric potentials are related by the Knight (1973) relation, which can be written in its linearized form as given by equation (11). Vogt and Haerendel (1998) have described the reflection of Alfvén waves in this case. They find that the reflection coefficient can be written in the same form as equation (58), but with a modified conductivity given by

$$\Sigma_{eff} = \frac{\Sigma_P}{1 + k_{\perp}^2 \lambda_{MI}^2} \quad (59)$$

where we have included the M-I coupling scale length defined by equation (45). Since the Pedersen conductivity is usually less than the Alfvén conductivity, the effect of this change is to reduce the magnitude of the reflection coefficient. In fact, the reflection coefficient will go to zero at a scale length

$$L_A^2 = \frac{\Sigma_A}{K} \frac{\Sigma_P}{\Sigma_P - \Sigma_A} \approx \frac{\Sigma_A}{K} \quad (60)$$

where the last approximate form holds for the usual case when  $\Sigma_P \gg \Sigma_A$ . This scale size is typically in the 10 km range. This scale length thus represents the point at which all of the Alfvén wave energy is absorbed. It is worth noting that for smaller scale sizes, the Alfvén wave is reflected from the acceleration region and does not even reach the ionosphere. Thus, narrow-scale Alfvén waves are decoupled from ionospheric drag, and may lead to enhanced flow in the outer magnetosphere.

## 2. Two-fluid model of shear Alfvén waves

When the perpendicular scale length of the Alfvén waves becomes too small, the ideal MHD approximation breaks down and additional terms in the generalized Ohm's Law must be included. In this case, the momentum equation (48) remains the same, but Faraday's Law must be modified to include the effects of parallel electric fields. Thus, (49) becomes:

$$\frac{\partial \mathbf{b}}{\partial t} = -c \left( \frac{\partial}{\partial z} (\hat{\mathbf{z}} \times \mathbf{E}_\perp) + \nabla_\perp \times \mathbf{E}_\parallel \right) \quad (61)$$

Let us consider the first term in this equation by using the ideal Ohm's Law to write:

$$-c \frac{\partial}{\partial z} (\hat{\mathbf{z}} \times \mathbf{E}_\perp) = B_0 \frac{\partial}{\partial z} (\hat{\mathbf{z}} \times (\mathbf{v} \times \hat{\mathbf{z}})) = B_0 \frac{\partial \mathbf{v}_\perp}{\partial z} \quad (62)$$

in agreement with the original form of (49). The parallel electric field can be determined from the generalized Ohm's Law:

$$E_z = \frac{m_e}{ne^2} \frac{\partial j_z}{\partial t} - \frac{1}{ne} \frac{\partial p_e}{\partial z} \quad (63)$$

where we have assumed an isotropic electron pressure. Note that the perpendicular electric field is not strongly affected by the non-ideal effects, since the  $\mathbf{v} \times \mathbf{B}$  electric field is dominant. We next must determine an equation for the electron pressure. In this model, the electron motion is predominantly along the magnetic field (with the exception of the  $\mathbf{E} \times \mathbf{B}$  drift, which doesn't have a divergence), and so, assuming isothermal electrons, the density change can be written as:

$$\frac{\partial \delta n}{\partial t} = -n_0 \frac{\partial v_z}{\partial z} = \frac{1}{e} \frac{\partial j_z}{\partial z} \quad (64)$$

Now we can write an equation for the time derivative of the parallel electric field:

$$\frac{\partial E_z}{\partial t} = \frac{m_e}{ne^2} \frac{\partial^2 j_z}{\partial t^2} - \frac{T_e}{ne^2} \frac{\partial^2 j_z}{\partial z^2} \quad (65)$$

The curl of this equation will give:

$$\begin{aligned} \frac{\partial}{\partial t} (\nabla_\perp \times \mathbf{E}_z) &= \frac{c}{\omega_{pe}^2} \frac{\partial^2}{\partial t^2} (\nabla_\perp \times (\nabla_\perp \times \mathbf{b})) - c \lambda_{De}^2 \frac{\partial^2}{\partial z^2} (\nabla_\perp \times (\nabla_\perp \times \mathbf{b})) \\ &= -\frac{c}{\omega_{pe}^2} \frac{\partial^2}{\partial t^2} \nabla_\perp^2 \mathbf{b} + c \lambda_{De}^2 \frac{\partial^2}{\partial z^2} \nabla_\perp^2 \mathbf{b} \end{aligned} \quad (66)$$

Let us now take the time derivative of (61), and use (62) and (66):

$$\begin{aligned} \frac{\partial^2 \mathbf{b}}{\partial t^2} &= B_0 \frac{\partial^2 \mathbf{v}}{\partial z \partial t} - c \frac{\partial}{\partial t} (\nabla_\perp \times \mathbf{E}_\parallel) \\ &= V_A^2 \frac{\partial^2 \mathbf{b}}{\partial z^2} + \frac{c^2}{\omega_{pe}^2} \frac{\partial^2}{\partial t^2} \nabla_\perp^2 \mathbf{b} - c^2 \lambda_D^2 \frac{\partial^2}{\partial z^2} \nabla_\perp^2 \mathbf{b} \end{aligned} \quad (67)$$

Now we have an equation for only the magnetic perturbation. If we Fourier analyze in the usual manner, the dispersion relation can be written as:

$$\omega^2 = k_\parallel^2 V_A^2 \frac{1 + k_\perp^2 \rho_s^2}{1 + k_\perp^2 \lambda^2} \quad (68)$$

where we introduce the electron inertial length,  $\lambda = c / \omega_{pe}$ , and the ion acoustic gyroradius,

$\rho_s = c\lambda_D/V_A = c_s/\Omega_i$ , where  $c_s = \omega_{pi}\lambda_D$  is the sound speed (recall that  $c/V_A = \omega_{pi}/\Omega_i$ ).

We may note a number of properties of this solution. First of all, it can be seen that there could be two different polarizations of this wave that have identical dispersion relations since (67) does not distinguish between perturbations in the  $x$  and  $y$  directions. The two-fluid effects also change the relationship between the various quantities. The relation between the velocity and magnetic field can be found from (48) and (68) to be:

$$\mathbf{v} = -\frac{B_0}{4\pi\rho} \frac{k_{\parallel}}{\omega} \mathbf{b} = \mp \frac{\sqrt{1+k_{\perp}^2\lambda^2}}{\sqrt{1+k_{\perp}^2\rho_s^2}} \frac{\mathbf{b}}{\sqrt{4\pi\rho}} \quad (69)$$

and similarly, the perpendicular electric field becomes:

$$\mathbf{E}_{\perp} = \pm \frac{V_A}{c} \sqrt{\frac{1+k_{\perp}^2\lambda^2}{1+k_{\perp}^2\rho_s^2}} \mathbf{b} \times \hat{\mathbf{z}} \quad (70)$$

This relationship between the electric and magnetic perturbations has been recently verified in Freja data by Stasiewicz et al. (2000). Equation (63) gives the parallel electric field in terms of the magnetic perturbation. Equation (70) can then be used to give the parallel electric field in terms of the perpendicular field:

$$\begin{aligned} E_{\parallel} &= \frac{c}{\omega_{pe}^2} \omega \mathbf{k}_{\perp} \times \mathbf{b} - \frac{ck_{\parallel}^2\lambda_D^2}{\omega} \mathbf{k}_{\perp} \times \mathbf{b} \\ &= \frac{c^2}{\omega_{pe}^2} \frac{1+k_{\perp}^2\rho_s^2}{1+k_{\perp}^2\lambda^2} k_{\parallel} \mathbf{k}_{\perp} \cdot \mathbf{E}_{\perp} - \rho_s^2 k_{\parallel} \mathbf{k}_{\perp} \cdot \mathbf{E}_{\perp} \\ &= -\frac{c^2}{\omega_{pe}^2} \frac{1+k_{\perp}^2\rho_s^2}{1+k_{\perp}^2\lambda^2} \frac{\partial}{\partial z} \nabla_{\perp} \cdot \mathbf{E}_{\perp} + \rho_s^2 \frac{\partial}{\partial z} \nabla_{\perp} \cdot \mathbf{E}_{\perp} \end{aligned} \quad (71)$$

Note that these expressions hold for both direction of propagation.

It may be noted that the first term in each of these expressions gives the electron inertial effect, while the second term gives the effect of finite electron pressure. It is interesting to note that the direction of the parallel electric field is different for these two cases. In the inertial limit, the parallel electric field acts to accelerate the electrons in the direction required to carry the field-aligned current, while it acts to retard the electrons in the warm plasma limit. It should be asked which of these two effects is most important. From the dispersion relation (68), it can be seen that the inertial effect is more important when  $\lambda$  is large, while the pressure effect is important when  $\rho_s$  is large. The ratio between these two terms is:

$$\frac{\rho_s}{\lambda} = \frac{c\lambda_D/V_A}{c/\omega_{pe}} = \frac{\sqrt{T_e/m_e}}{V_A} = \sqrt{\beta} \frac{m_i}{m_e} \quad (72)$$

where in the last line we have defined the plasma  $\beta = 4\pi n T_e / B_0^2$ . Thus, in cold and strongly magnetized plasmas, the electron inertial length is dominant, while in warm or more weakly magnetized plasmas, the electron pressure is the most important effect. Lysak and Carlson (1981) showed that on auroral field lines, the region below about 4-5  $R_E$  is inertia dominated, while above that altitude the pressure dominates. More recently, Lysak and Lotko (1996) have considered the same question using a slightly different profile with a similar conclusion.

Physically, equation (72) shows that the pressure effect is dominant when the electron thermal speed is greater than the Alfvén speed, i.e., when the Landau resonance of the Alfvén

wave is well within the bulk of the electron distribution. Conversely, in the inertia dominated regime the electron Landau resonance is far out on the tail of the distribution. From the dispersion relation (68), it can be seen that the pressure effect increases the wave phase speed while the inertia effect decreases it; thus, roughly speaking, it could be said that the electrons accelerate the wave in the pressure regime and that electron inertia effects slow down the Alfvén wave in the cold regime. It may be noted that in the inertial regime, the electrons act as a cold fluid to the Alfvén wave and can be accelerated in bulk. It can be said that in this regime, the Alfvén wave carries a parallel electric field in order to accelerate the electrons up to the point where they can carry the current required by the Alfvén wave.

### 3. Kinetic theory of the Alfvén wave

The fluid model described above does not take Landau damping into account, and does not describe the dispersion relation accurately in the transition region between the two regimes. Thus, we need to examine the full kinetic Alfvén wave dispersion relation, and to attempt to evaluate the importance of the kinetic effects on the propagation of the wave. The following derivation of the kinetic Alfvén wave dispersion relation is taken from a recent paper by Lysak and Lotko (1996).

The starting point for any linear kinetic theory of electromagnetic waves in a plasma begins with finding the determinant of the  $3 \times 3$  matrix equation that arises from the coupled Vlasov-Maxwell system. For low frequency ( $\omega \ll \Omega_i$ ) waves in an isotropic plasma in which  $k_{\perp}^2 \rho_i^2 \ll 1$  and  $k_{\perp}^2 \rho_s^2 \ll 1$ , the solution to this equation yields the three MHD wave modes, which in a low- $\beta$  plasma can be written as the fast mode,  $\omega^2 = k^2 V_A^2 + k_{\perp}^2 c_s^2$ , the shear Alfvén mode,  $\omega = k_{\parallel} V_A$ , and the slow, or ion acoustic mode,  $\omega = k_{\parallel} c_s$ . When large perpendicular wave number is assumed, the fast mode decouples from the others since  $\omega_{fast} > k_{\perp} V_A = k_{\perp} \rho_s \Omega_i (V_A / c_s)$ , which is greater than the ion gyrofrequency when  $k_{\perp} \rho_s > c_s / V_A = \sqrt{\beta}$  (Hasegawa and Uberoi, 1982). The kinetic Alfvén wave is then the result of the coupling between the shear Alfvén mode and the ion acoustic mode. Considering only the regime  $\beta \ll 1$ , we find to first order that the ion response is primarily perpendicular to the background magnetic field, while the electron response is predominantly parallel. Then the dispersion relation for the kinetic Alfvén wave is given by the determinant of the  $2 \times 2$  matrix:

$$\det \begin{pmatrix} \frac{c^2}{V_A^2} \frac{1 - \Gamma_0(\mu_i)}{\mu_i} - n_{\parallel}^2 & n_{\parallel} n_{\perp} \\ n_{\parallel} n_{\perp} & \frac{\Gamma_0(\mu_e)}{k_{\parallel}^2 \lambda_{De}^2} (1 + \xi Z(\xi)) - n_{\perp}^2 \end{pmatrix} = 0 \quad (73)$$

In this dispersion relation, it has been assumed that  $c^2 / V_A^2 \gg 1$  and that  $k_{\parallel}^2 \lambda_{De}^2 \ll 1$ , so that the unit terms in the diagonal elements can be dropped. Here  $n_{\parallel} = k_{\parallel} c / \omega$ ,  $n_{\perp} = k_{\perp} c / \omega$ ,  $\mu_i = k_{\perp}^2 \rho_i^2$ ,  $\mu_e = k_{\perp}^2 \rho_e^2$ ,  $\xi = \omega / k_{\parallel} a_e$ , and  $a_e = \sqrt{2T_e / m_e}$ ,  $\Gamma_0$  is the modified Bessel function  $\Gamma_0(\mu) = e^{-\mu} I_0(\mu)$ , and  $Z$  is the usual plasma dispersion function (Fried and Conte, 1961). Definitions of other symbols in equation (73) and a detailed derivation of this equation are given in Lysak and Lotko

(1996).

The solution to this dispersion relation can be written as:

$$\left(\frac{\omega}{k_{\parallel}V_A}\right)^2 = \frac{\mu_i}{1-\Gamma_0(\mu_i)} + \frac{k_{\perp}^2\rho_s^2}{\Gamma_0(\mu_e)[1+\xi Z(\xi)]} \quad (74)$$

Note that for small ion gyroradius, we have  $\Gamma_0(\mu_i) \approx 1 - \mu_i + (3/4)\mu_i^2$ , and so we have:

$$\frac{\mu_i}{1-\Gamma_0(\mu_i)} \approx \frac{1}{1-(3/4)\mu_i} \approx 1 + \frac{3}{4}\mu_i \quad (75)$$

Also note that for hot electrons,  $\xi \ll 1$ , and for small electron gyroradius,  $\Gamma_0(\mu_e) \approx 1$ ; thus, the denominator of the second term of equation (74) is approximately unity. Therefore, in the hot electron and small ion gyroradius limits, we have:

$$\left(\frac{\omega}{k_{\parallel}V_A}\right)^2 \approx 1 + k_{\perp}^2 \left( \rho_s^2 + \frac{3}{4}\rho_i^2 \right) \quad (76)$$

This expression is in agreement with the warm plasma limit of equation (68), with the addition of an additional term due to the ion gyroradius effect that was not included in the two-fluid picture.

For cold electrons, the electron gyroradius can again be ignored and we can write  $1 + \xi Z(\xi) \approx -1/2\xi^2 = -(k_{\parallel}v_e/\omega)^2$ , where we define  $v_e^2 = T_e/m_e = a_e^2/2$ . Thus, we can write (74) as:

$$\begin{aligned} \left(\frac{\omega}{k_{\parallel}V_A}\right)^2 &= \frac{\mu_i}{1-\Gamma_0(\mu_i)} - \left(\frac{\omega}{k_{\parallel}v_e}\right)^2 k_{\perp}^2\rho_s^2 \\ &= \frac{\mu_i}{1-\Gamma_0(\mu_i)} - \left(\frac{\omega}{k_{\parallel}V_A}\right)^2 \frac{k_{\perp}^2c^2}{\omega_{pe}^2} \end{aligned} \quad (77)$$

which becomes:

$$\left(\frac{\omega}{k_{\parallel}V_A}\right)^2 = \frac{\mu_i}{1-\Gamma_0(\mu_i)} \frac{1}{1+k_{\perp}^2c^2/\omega_{pe}^2} \quad (78)$$

This result reduces to the cold plasma limit of equation (68) when the ion gyroradius is taken to be zero, in which case the first factor is 1. Thus, the hot and cold limits of the fluid dispersion relation follow from equation (74).

The real part of the dispersion relation for the kinetic Alfvén wave has been plotted in Figure 1 of Lysak and Lotko (1996) as contours of the parallel phase velocity  $\omega/k_{\parallel}V_A$  as a function of the normalized perpendicular wave number  $k_{\perp}c/\omega_{pe}$  and a parameter proportional to the electron pressure  $v_e^2/V_A^2 = \beta m_i/m_e$ . Note that the value  $\beta = m_e/m_i$  denotes the boundary between the kinetic and the inertial regimes. Figure 1a shows the results based on the fluid theory given by equation (68) with zero ion temperature, while the other 3 panels of the Figure show results from solutions of the full dispersion relation given by (74) for ion-to-electron temperature ratios of 0, 1, and 10. It can be seen from these figures that the basic topology of the fluid dispersion relation is preserved by the kinetic dispersion relation, with the boundary between kinetic and inertial type of dispersion occurring approximately at the point

where  $v_e^2(1+3T_i/4T_e) \approx V_A^2$ . At this point, the numerator and denominator in the fluid dispersion relation given by equation (68) are equal, and the phase velocity is exactly the Alfvén speed. Note that the phase velocity increases more strongly with increased perpendicular wave number for higher ion temperature.

Figure 2 of Lysak and Lotko (1996) shows the Landau damping rates, normalized to the wave frequency, for the three kinetic cases considered (of course, the damping in the fluid model is zero). It is interesting to note that there is not a strong enhancement in the Landau damping rate at  $v_e = V_A$ , as might be expected, but rather the damping rate for a given  $k_\perp c / \omega_{pe}$  increases monotonically with increasing electron temperature. For a given value of  $T_i/T_e$ , the damping rate is basically a function of  $k_\perp \rho_s$  at lower electron temperature. For the higher electron temperature regime, the damping rate becomes nearly independent of the electron temperature and is just a function of  $k_\perp c / \omega_{pe}$  until the electron gyroradius effect becomes important. It may be noted that the damping rate is less than about 0.1 of the wave frequency whenever the wave number satisfies both  $k_\perp \rho_s < 1$  and  $k_\perp c / \omega_{pe} < 1$ . The other clear point from these plots is that the damping rate is suppressed by high ion temperatures, which may seem surprising at first glance.

This result is due to the ion effects on the dispersion, as can be seen by considering the behavior of the parameter  $\xi = \omega / k_\parallel a_e$ . This parameter is the important parameter for the Landau damping term, since for weak damping the damping rate will be proportional to  $\xi e^{-\xi^2}$ , a function that maximizes at  $\xi = 1/\sqrt{2} \approx 0.7$ . For  $T_i = 0$ , this maximum point does indeed occur for  $v_e^2 \approx V_A^2$ , but for higher ion temperatures, the  $\xi = 0.7$  value is confined to regions in which  $k_\perp c / \omega_{pe} < 1$ , which are associated with small damping rates. Thus, the ion dispersion minimizes electron Landau damping by moving the Landau resonance point into the tail of the electron distribution when the perpendicular wave number is large.

In order to determine the polarization characteristics of the kinetic Alfvén wave, we should consider the dispersion relation of (124) in more detail. Recall that this expression is really the solution to the matrix equation:

$$\begin{pmatrix} \epsilon_\perp - n_\parallel^2 & n_\parallel n_\perp \\ n_\parallel n_\perp & \epsilon_\parallel - n_\perp^2 \end{pmatrix} \begin{pmatrix} E_x \\ E_z \end{pmatrix} = 0 \quad (79)$$

where the dielectric tensor elements are:

$$\epsilon_\perp = \frac{c^2}{V_A^2} \frac{1 - \Gamma_0(\mu_i)}{\mu_i} \quad \epsilon_\parallel = \frac{\Gamma_0(\mu_e)}{k_\parallel^2 \lambda_{De}^2} [1 + \xi Z(\xi)] \quad (80)$$

The wave polarization characteristics can be found from the first row of equation (79):

$$\frac{E_z}{E_x} = \frac{n_\parallel^2 - \epsilon_\perp}{n_\parallel n_\perp} = \frac{n_\parallel}{n_\perp} \left( 1 - \frac{\epsilon_\perp}{n_\parallel^2} \right) \quad (81)$$

while the magnetic perturbation can be written using Faraday's law

$$B_y = n_\parallel E_x - n_\perp E_z = \frac{\epsilon_\perp}{n_\parallel} E_x \quad (82)$$

Full numerical solutions of these expressions can be found in Lysak (1998). The field ratios given by equation (82) has been used together with Polar data by Wygant et al. (2001) in

order to estimate the perpendicular wavelength of strong Alfvénic fluctuations at the plasma sheet boundary layer. These authors then used this perpendicular wavelength to estimate the parallel potential of the wave by using equation (81). These results were consistent with the energy of counterstreaming field-aligned electrons observed by the spacecraft. In addition, there was an asymmetry in the electron distribution, with more electrons going in the direction of the wave propagation. It has been suggested that this tail represents the Landau resonant tail of the electron distribution.

To evaluate these expressions analytically, it is useful to note that the dispersion relation (73) can be written in the form:

$$n_{\parallel}^2 = \frac{\varepsilon_{\perp}(\varepsilon_{\parallel} - n_{\perp}^2)}{\varepsilon_{\parallel}} \quad (83)$$

Let us consider this expression in the cold and hot electron limits. For cold electrons, we have  $\varepsilon_{\parallel} = -\omega_{pe}^2/\omega^2$ . In this case, equation (83) can be evaluated to find:

$$n_{\parallel}^2 = \varepsilon_{\perp}(1 + k_{\perp}^2\lambda^2) \quad (84)$$

Inserting this expression into (81), we can write:

$$\frac{E_z}{E_x} = \frac{k_{\parallel}k_{\perp}\lambda^2}{1 + k_{\perp}^2\lambda^2} \quad (85)$$

Note that although this expression includes the full ion gyroradius effect, this does not enter into the expression for the parallel electric field. It is also worth noting that for very short perpendicular wavelength,  $k_{\perp}\lambda \gg 1$ , the wave becomes electrostatic, i.e.,  $E_{\parallel}/E_{\perp} = k_{\parallel}/k_{\perp}$ . The magnetic field ratio in this case becomes:

$$\frac{B_y}{E_x} = \frac{c}{V_A} \sqrt{\frac{(1 - \Gamma_0)/\mu_i}{1 + k_{\perp}^2\lambda^2}} \quad (86)$$

Note that since  $(1 - \Gamma_0)/\mu$  is a function that decreases from 1 to 0 with increasing  $\mu$ , both the ion gyroradius and electron inertial effects decrease the magnetic field from the ideal MHD value.

In the hot electron limit,  $\varepsilon_{\parallel} = 1/k_{\parallel}^2\lambda_D^2$ , and the solution to the dispersion relation can be written as:

$$n_{\parallel}^2 = \frac{(c^2/V_A^2)(1 - \Gamma_0)/\mu_i}{1 + k_{\perp}^2\rho_s^2(1 - \Gamma_0)/\mu_i} \quad (87)$$

In this case, inserting this expression into (81) yields:

$$\frac{E_z}{E_x} = -k_{\parallel}k_{\perp}\rho_s^2 \frac{1 - \Gamma_0}{\mu_i} \quad (88)$$

Note that this parallel electric field primarily depends on the electron pressure effect; in fact, finite ion gyroradius reduces the parallel electric field. It is sometimes mistakenly stated that the ion gyroradius effect causes the parallel electric field in kinetic Alfvén waves. It can be seen from equations (85) and (88) that this is not the case, and that it is electron inertia and pressure that give rise to the parallel electric field. In the warm plasma limit, the magnetic perturbation satisfies:

$$\frac{B_y}{E_x} = \frac{c}{V_A} \sqrt{\frac{1-\Gamma_0}{\mu_i} \left( 1 + k_{\perp}^2 \rho_s^2 \frac{1-\Gamma_0}{\mu_i} \right)} \quad (89)$$

An interesting special case of this dispersion relation occurs in the regime where  $\beta \ll m_e/m_i$ , but with the ion gyroradius being large, so that  $\mu_i \gg 1$  applies. In this situation, the function  $\Gamma_0(\mu_i)$  goes to zero. If we also assume that  $k_{\perp}c/\omega_{pe} \gg 1$ , then equation (78) reduces to:

$$\omega^2 = k_{\parallel}^2 V_A^2 \frac{k_{\perp}^2 \rho_i^2}{k_{\perp}^2 c^2 / \omega_{pe}^2} = k_{\parallel}^2 \frac{T_i}{m_e} \quad (90)$$

Note that in this case, the dependence of the frequency on the perpendicular wave number goes away, and so the wave propagates strictly parallel to the field. This wave is called an ‘‘electron acoustic wave,’’ since its dispersion relation is like that of the ion acoustic wave, but with the roles of electrons and ions reversed. This situation arises since for very short perpendicular wavelength, the ions become demagnetized and act as an equilibrium Boltzmann population, while the electrons are a cold fluid restricted to moving along the magnetic field. This wave is strongly damped unless the ions are much hotter than the electrons, since for comparable temperature this wave has a parallel phase velocity equal to the electron thermal speed. Such a situation can arise in the auroral zone in when the ions have already been heated by wave-particle interactions. Evidence for such waves has been seen on the Freja satellite at 1700 km altitude in the auroral zone (Boehm et al., 1995; Seyler and Wahlund, 1996).

#### 4. The ionospheric Alfvén resonator

We have already introduced the idea that the ionospheric conductivity can affect auroral current systems, both in the electrostatic picture and in the reflection of Alfvén waves. By assuming that the ionosphere is a uniform slab, we showed that only the height-integrated Pedersen conductivity was significant. Now we would like to develop a more realistic model of the ionosphere that can deal with the horizontal and vertical structure of the ionospheric parameters. We will do this in three parts: first, we will consider the parallel inhomogeneities in the Alfvén speed, which give rise to a resonant cavity sometimes referred to as the ionospheric Alfvén resonator. Secondly, we will treat the time variations of the ionosphere as the result of the electron precipitation that can change the ionospheric conductivity. Finally, we will take into account the vertical structure of the ionospheric conductivity, relaxing the assumption that the ionosphere is a height-integrated slab. This will allow a discussion of the propagation of Alfvén waves through the ionosphere and atmosphere and down to the ground.

Our previous analyses of the reflection of Alfvén waves from the ionosphere assumed that the Alfvén speed, and equivalently the Alfvén conductivity, was constant along the field line. Except for the special case where the density scales as the square of the magnetic field, this is not in general true, and there are Alfvén speed gradients. If these gradients are weak enough, WKB theory may be used to follow the propagation of the Alfvén waves. This situation may apply in the outer magnetosphere, but in the inner magnetosphere, the Alfvén speed gradient may become steep enough so the WKB theory is not valid. In such a circumstance, the Alfvén wave may be reflected by the gradient in the Alfvén speed.

To illustrate this reflection, consider the extreme case of a discontinuity in the Alfvén speed. If the wave is incident from the side with Alfvén speed  $V_{A1}$ , and is transmitted to the side

with speed  $V_{A2}$ , then an argument analogous to that for the ionospheric reflection yields:

$$R = \frac{E_{ref}}{E_{inc}} = \frac{\Sigma_{A1} - \Sigma_{A2}}{\Sigma_{A1} + \Sigma_{A2}} \quad (91)$$

Thus, propagation into increasing Alfvén speed (decreasing Alfvén conductivity) leads to an enhancement of the wave electric field and a decrease in the magnetic field, and vice versa. This model has been used to calculate the propagation of Alfvén waves in inhomogeneous media by Mallinckrodt and Carlson (1978).

In general, as noted above, a strong inhomogeneity in the Alfvén speed implies that we cannot use the WKB approximation and that we need to solve the complete wave equation for the wave fields. In the topside ionosphere, there is such a strong inhomogeneity due to the sharp exponential decrease in the plasma density with increasing altitude above a few hundred kilometers. This decrease takes place with a typical scale height of less than 1000 km. Since the magnetic field varies only weakly on such spatial scales, the Alfvén speed increases exponentially with a comparable scale height above the ionosphere. Above about 6000 km altitude, the density decrease becomes more gradual, and the decrease in the magnetic field leads to a slow decrease in the Alfvén speed.

In order to analyze the eigenmodes of this system, it is useful to use a formulation of the Alfvén wave equations using scalar and vector potentials. The fundamental starting point of the analysis is the Maxwell equations in a dielectric medium:

$$\frac{\partial \mathbf{B}}{\partial t} = -c \nabla \times \mathbf{E} \quad (92)$$

$$\frac{\partial}{\partial t} (\bar{\epsilon} \cdot \mathbf{E}) = c \nabla \times \mathbf{B} \quad (93)$$

It is useful here to introduce vector and scalar potentials in the usual way by  $\mathbf{B} = \nabla \times \mathbf{A}$  and  $\mathbf{E} = -\nabla \Phi - (1/c) \partial \mathbf{A} / \partial t$ . If we restrict the analysis to transverse waves with  $\delta B_z = 0$ , where  $\delta B_z$  is the perturbation in the component of  $\mathbf{B}$  parallel to the background field, we can describe the magnetic perturbation totally by the  $z$  component of the vector potential. This implies that the perpendicular electric field is described totally by the perpendicular gradient in the scalar potential  $\mathbf{E}_\perp = -\nabla_\perp \Phi$ . If we assume the ideal MHD case, so that the parallel electric field goes to zero, we can write:

$$\frac{\partial A_z}{\partial t} = -c \frac{\partial \Phi}{\partial z} \quad (94)$$

The system must be closed by a gauge condition. The appropriate gauge condition for this case is the macroscopic analogue of the Lorentz gauge:

$$\frac{\partial (\epsilon_\perp \Phi)}{\partial t} + c \nabla \cdot \mathbf{A} = 0 \quad (95)$$

Note that we use the perpendicular component of the dielectric tensor since the scalar potential is directly related to the perpendicular electric field. Inserting  $\epsilon_\perp \approx c^2 / V_A^2$  and noting that only the parallel component of the vector potential is non-zero, equation (3) becomes:

$$\frac{\partial \Phi}{\partial t} = -\frac{V_A^2}{c} \frac{\partial A_z}{\partial z} \quad (96)$$

It is easily verified that the perpendicular gradient of equation (96) yields the electric field equation (93).

Equations (94) and (96) then represent a complete set of equations describing the shear mode Alfvén wave. The inhomogeneity of the flux tube enters through the Alfvén speed in (96). In order to simplify the problem to the point where we can find analytic solutions, we shall adopt the simple profile (Greifinger and Greifinger, 1968; Trakhtengertz and Feldstein, 1984):

$$V_A^2(z) = \frac{V_{AI}^2}{\varepsilon^2 + e^{-z/h}} \quad (97)$$

where  $V_{AI}$  is the Alfvén speed at the ionospheric altitude,  $h$  is the ionospheric scale height, and  $\varepsilon$  is a small parameter. Here it should be recognized that the coordinate  $z$  increases in the upward direction, in contrast with our previous discussion in which  $z$  was in the direction of the magnetic field. Note that at high altitudes,  $z \gg h$ , the Alfvén speed simply becomes  $V_{AM} = V_{AI} / \varepsilon$ . Thus the smallness of the parameter  $\varepsilon$  represents the fact that the Alfvén speed in the magnetosphere is much larger than that in the ionosphere. Note that while the density profile given by (97) does not take into account the decrease of the Alfvén speed at high altitudes, it does give a reasonable representation of the Alfvén speed profiles in the region above the ionosphere.

The system given by (94) and (96) with the Alfvén speed profile (97) can be analyzed for its eigenmodes by Fourier transforming in time and in the perpendicular dimensions, leading to the wave equation:

$$\frac{\partial^2 \Phi}{\partial z^2} + \frac{\omega^2}{V_{AI}^2} (\varepsilon^2 + e^{-z/h}) \Phi = 0 \quad (98)$$

This equation can be transformed by switching to the independent variable  $x = x_0 e^{-z/2h}$ , where  $x_0 = 2h\omega/V_{AI}$ . This transformation leads to the equation:

$$x^2 \frac{d^2 \Phi}{dx^2} + x \frac{d\Phi}{dx} + (x^2 + x_0^2 \varepsilon^2) \Phi = 0 \quad (99)$$

This equation can be recognized as being Bessel's equation; however, in the ordinary form of Bessel's equation:

$$x^2 \frac{d^2 w}{dx^2} + x \frac{dw}{dx} + (x^2 - \nu^2) w = 0 \quad (100)$$

it can be seen that the square of the order enters with a minus sign. Thus, in this case, the Bessel function solutions have an imaginary order, and the solutions to the wave equation take on the form:

$$\Phi = A^+ J_{ix_0 \varepsilon}(x) + A^- J_{-ix_0 \varepsilon}(x) \quad (101)$$

It can be shown (Lysak, 1991) that these two solutions correspond to the downgoing and upgoing waves, respectively. This follows from considering the large  $z$  limit of the Bessel functions, which corresponds to  $x \ll 1$ . In this limit:

$$\Phi^\pm \equiv J_{\pm ix_0 \varepsilon}(x) \approx \frac{(x/2)^{\pm ix_0 \varepsilon}}{\Gamma(1 \pm ix_0 \varepsilon)} \quad (102)$$

where  $\Gamma$  is the gamma function (not the modified Bessel function as before). Writing this in terms of the original variable  $z$  we find that

$$\Phi^\pm \propto e^{\mp i(x_0 \varepsilon / 2h)z - i\omega t} = e^{-i\omega(t \pm z/V_{AM})} \quad (103)$$

where we have inserted the time dependent phase factor  $e^{-i\omega t}$  implied by our Fourier transformation. Equation (11) shows that the two solutions are down and upgoing plane waves at large altitudes.

Determination of the eigenfrequencies for these waves requires the application of the boundary condition at the ionosphere. Noting that the field-aligned current can be written as:

$$j_z = \frac{c}{4\pi} (\nabla \times \mathbf{B})_z = -\frac{c}{4\pi} \nabla_{\perp}^2 A_z \quad (104)$$

If we now insert this into equation (1.36), noting that there is a sign change due to changing the direction of the  $z$  coordinate, the ionospheric boundary condition becomes:

$$\nabla_{\perp}^2 \left( \frac{c}{4\pi} A_z + \Sigma_p \Phi \right) = 0 \quad (105)$$

The Fourier transform in time of equation (10) implies that:

$$A_z = -\frac{ic}{\omega} \frac{d\Phi}{dz} = \frac{ic}{V_{Al}} \frac{x}{x_0} \Phi' \quad (106)$$

where  $\Phi' = d\Phi/dx$ , and evaluating the condition (105) at the ionosphere, which corresponds to  $x = x_0$ , we can write:

$$i\Phi' + \alpha\Phi = 0 \quad (107)$$

where  $\alpha = \Sigma_p / \Sigma_{Al}$  measures the Pedersen conductivity in units of the Alfvén conductivity at the ionosphere. The boundary condition (107) can be considered to be an eigenvalue equation for the parameter  $x_0$ , which is essentially the mode frequency scaled by the fundamental frequency in the problem, which is  $V_{Al}/2h$ . The upper boundary condition can be taken to be a radiation boundary condition, which picks out the  $J_{i\nu, \varepsilon}$  solution for inward propagating waves and the  $J_{-i\nu, \varepsilon}$  solution for outward propagating waves. It can be easily seen that the solutions are parameterized by  $\varepsilon$ , which is always much smaller than one, and  $\alpha$ , which may be small or large.

The eigenvalue equation (107) can be easily solved in the limits of high and low conductivity. First, note that for  $x_0\varepsilon \ll 1$ , the Bessel function solutions can be expanded in order, noting that the derivative of  $J_\nu(x)$  with respect to  $\nu$  evaluated for  $\nu = 0$  is  $(\pi/2)Y_0(x)$  (Abramowitz and Stegun, 1964, equation 9.1.68). Thus, the solutions can be written:

$$J_{\pm i\nu, \varepsilon}(x) \approx J_0(x) \pm \frac{ix_0\varepsilon\pi}{2} Y_0(x) \quad (108)$$

When the scaled conductivity  $\alpha \rightarrow 0$ , the second term in (107) can be ignored, and the eigenvalue condition just yields  $\Phi' = 0$ . Thus, to lowest order the eigenvalues are given by  $x_0 = j_{1,s}$ , where the values  $j_{1,s}$  are the zeroes of  $J_1(x)$ , since  $J_1$  is the negative of the derivative of  $J_0$ . To first order in the small parameters  $\alpha$  and  $\varepsilon$ , it can be easily seen that the scaled eigenfrequency yields  $x_0 = j_{1,s} + i\eta$ , where  $\eta = \mp j_{1,s}\varepsilon(\pi/2)Y_1(j_{1,s})/J_0(j_{1,s})$ . Note that  $\eta$  is proportional to the growth rate,  $\eta = 2h\gamma/V_{Al}$ . Note here that  $Y_1$  and  $J_0$  always have opposite sign when  $J_1$  is zero, since by a Wronskian condition:

$$J_1(z)Y_0(z) - J_0(z)Y_1(z) = \frac{2}{\pi z} \quad (109)$$

(Abramowitz and Stegun, 1964, equation 9.1.16). Thus, the incoming solution has a positive growth rate, since energy is entering the system, while the outgoing solution is damped.

In the limit of high conductivity,  $\alpha \gg 1$ , the derivative term in (107) is negligible, and the eigenvalues are now the zeroes of  $J_0$ . Expansion to the next higher order yields:

$$\eta = -\frac{1}{\alpha} \pm \frac{\pi}{2} j_{0,s} \varepsilon \frac{Y_0(j_{0,s})}{J_1(j_{0,s})} \quad (110)$$

where by equation (109) we have  $Y_0 / J_1 > 0$  when evaluated at a zero of  $J_0$ . Thus again the incoming solution has a positive growth rate while the outgoing solution is damped. For arbitrary values of the conductivity, the eigenfrequencies make a transition from the zeroes of  $J_1$  to the zeroes of  $J_0$  as the conductivity is increased. The transition takes place at  $\alpha \sim 1$ , which also corresponds to the maximum damping of both modes. This is not surprising since it corresponds to the point where the Alfvén conductivity at the ionosphere matches the ionospheric conductivity, which corresponds to no reflection in the uniform case as we saw earlier.

This effective resonant cavity also influences the reflection coefficient of Alfvén waves on auroral field lines. The reflection coefficient may be defined as the ratio of the amplitudes of the upgoing wave to the downgoing wave,  $R = A^- / A^+$ . This ratio must be determined by applying the boundary condition (107) to the combined wave solution at the ionosphere (i.e., at  $x = x_0$ ). This condition implies:

$$R = \frac{A^-}{A^+} = -\frac{iJ'_{ix,\varepsilon}(x_0) + \alpha J_{ix,\varepsilon}(x_0)}{iJ'_{-ix,\varepsilon}(x_0) + \alpha J_{-ix,\varepsilon}(x_0)} \quad (111)$$

This relation has been calculated numerically for a number of cases by Lysak (1991). This relationship reduces to the usual condition (58) in the limit of low frequencies,  $x_0 \ll 1$ . In this limit, it can be seen by expanding (109) for small argument that  $J_{\pm ix,\varepsilon}(x_0) \approx 1$  and  $J'_{\pm ix,\varepsilon}(x_0) \approx \pm i\varepsilon$ , so that  $R \approx (\varepsilon - \alpha) / (\varepsilon + \alpha) = (\Sigma_{AM} - \Sigma_{AI}) / (\Sigma_{AM} + \Sigma_{AI})$ , as in the uniform case. At these very low frequencies, the wavelength of the Alfvén wave is so long that it effectively does not see the cavity. On the other hand, for very large frequencies, the numerical results suggest that  $R \rightarrow (1 - \alpha) / (1 + \alpha) = (\Sigma_{AI} - \Sigma_P) / (\Sigma_{AI} + \Sigma_P)$ . (It would seem that an analytic result of this limit should be possible to find; however, this would involve the uniform asymptotic expansions of the Bessel functions, which are quite complicated.) This high frequency limit corresponds to the case where WKB theory is valid, and thus the reflection coefficient is described by the ionospheric Alfvén speed, rather than that in the magnetosphere.

In general, the reflection coefficient shows features at the resonant frequencies of the cavity. When the cavity is very deep (i.e.,  $\varepsilon$  very small) and the conductivity is high, the reflection coefficient shows a sharp decrease at the resonant frequencies. This may be interpreted in terms of the trapping of the wave in the cavity, so that, after multiple interactions with the ionosphere, the wave is eventually absorbed. When  $\varepsilon$  is not so low, e.g.,  $\varepsilon \sim 0.1$ , these features can still be seen, although they are not so sharp. When the conductivity is lower, the wave does not reflect as strongly; however, in this case the presence of the cavity can lead to an enhancement of the reflection compared with the low frequency limit, which may be interpreted in terms of a direct reflection of the wave from the Alfvén speed gradient above the ionosphere.

Although this model was calculated using the ideal MHD approximation, it is an easy matter to introduce the two-fluid effects. First of all, it can be noted that the strong gradients in the Alfvén speed occur at low altitudes, where the electron inertial effect is dominant. This effect implies that the parallel electric field is given by the first term in (63):

$$E_z = \frac{m_e}{ne^2} \frac{\partial j_z}{\partial t} = -\frac{c}{\omega_{pe}^2} \frac{\partial}{\partial t} \nabla_{\perp}^2 A_z \quad (112)$$

where the last step introduces the vector potential as in (4). Writing this parallel electric field in terms of the scalar and vector potentials in the usual way modifies equation (129) to read:

$$(1 - \lambda^2 \nabla_{\perp}^2) \frac{\partial A_z}{\partial t} = -c \frac{\partial \Phi}{\partial z} \quad (113)$$

where  $\lambda = c/\omega_{pe}$  as before. In Fourier space, this equation can be written as:

$$\frac{\partial \Phi}{\partial z} = \frac{i\omega}{c} (1 + k_{\perp}^2 \lambda^2) A_z \quad (114)$$

Combining this relationship with equation (62), we can generalize equation (66) to read:

$$\frac{d}{dz} \left[ \frac{1}{1 + k_{\perp}^2 \lambda^2(z)} \frac{d\Phi}{dz} \right] + \frac{\omega^2}{V_A^2(z)} \Phi = 0 \quad (115)$$

This equation does not have analytic solutions in general, but numerical solutions have been presented (Lysak, 1993). Note that the profiles of the Alfvén speed and of the electron inertial length are important in equation (67). In fact, even the perpendicular wave number should be considered to be a function of  $z$  since it will change due to the changing size of the flux tube, indicating roughly that  $k_{\perp}^2 \propto B_0$ . The results of Lysak (1993) were obtained by integrating equations (48) and (68) up from the ionosphere, starting with the ionospheric boundary condition (4). The resulting solution was then decomposed into incoming and outgoing wave solutions at the assumed upper boundary, and the reflection coefficient could be determined by their ratio. More recently, Lysak (1997) has presented solutions for the wave polarization by constructing the  $B_y / E_x$  ratio (or equivalently,  $A_z / \Phi$  ratios) in order to make comparisons with spacecraft data.

It is interesting to consider the behavior of the compressional MHD mode in the presence of the ionospheric Alfvén resonator discussed previously. The compressional MHD mode propagates isotropically in a cold plasma, with the wave equation given by

$$\frac{\partial^2 B_z}{\partial t^2} - V_A^2 \nabla^2 B_z = 0 \quad (116)$$

If we Fourier transform in time and in the perpendicular coordinate, and adopt the profile given by equation (97) for the Alfvén speed, then we find:

$$\frac{\partial^2 B_z}{\partial z^2} + \frac{\omega^2}{V_{Al}^2} (\epsilon^2 + e^{-z/h}) B_z = k_{\perp}^2 B_z \quad (117)$$

It may be noted that this equation is identical to equation (98) if the right hand side is set to zero. Equation (117) may be solved by the same coordinate transformation, with the result that the magnetic field perturbation can be written as  $B_z \sim J_{\pm\nu}(x)$ , where  $x$  is defined as in equation (99) but with  $\nu = \sqrt{4k_{\perp}^2 h^2 - x_0^2 \epsilon^2}$ . Note that the solution (101) corresponds to  $k_{\perp} \rightarrow 0$ . The order  $\nu$  becomes real when  $k_{\perp} > x_0 \epsilon / 2h = \omega / V_{AM}$ . Performing the expansion for  $z \rightarrow \infty$ , i.e.,  $x \ll 1$ , as in (102) we see that:

$$J_{\pm\nu}(x) \approx \frac{(x/2)^{\pm\nu}}{\Gamma(1 \pm \nu)} \propto e^{\mp\nu z / 2h} \quad (118)$$

Thus we see that real  $v$  corresponds to the evanescent solutions found for a uniform Alfvén speed when  $k_{\perp} > \omega / V_A$ . Note that we also could have the interesting situation that  $V_{Al} < \omega / k_{\perp} < V_{AM}$ . In this case, the magnetosonic wave can propagate close to the ionosphere where the Alfvén speed is low, but is evanescent at higher altitudes. This situation effectively traps the magnetosonic wave in the topside ionosphere, and the magnetosonic wave can then transport wave energy perpendicular to the field line through this cavity. The consequences of this type of cavity have been explored by Greifinger and Greifinger (1968), Fraser (1975), Fujita (1988) and Fujita and Tamao (1988). Recent modeling of the coupling between the shear and compressional modes has been given by Lysak (1997, 1999) in two dimensions and Lysak and Song (2001) in three dimensions.

#### D. Wave-Particle Interactions in the Auroral Zone

Auroral particle distributions such as those given in Figures 1 and 2 contain a number of features that can potentially give rise to instabilities. Strong gradients in the distribution function are likely to occur at each of the phase space boundaries. For the electrons, a beam of magnetospheric electrons can occur in the downgoing loss cone region. In practice, the region just inside the acceleration ellipse is filled with backscattered ionospheric electrons. These electrons reduce the positive slope in the distribution function, but there is generally still a positive slope in the electron distribution at the location of this ellipse. The electron distribution can also contain strong perpendicular gradients at the loss cone boundary as well as gradients in the trapped population that can also give rise to instabilities. For ions, the upgoing ion beams are the strongest source of free energy for plasma instabilities, but the ion loss cone can also contribute.

##### 1. Beam-driven instabilities

There are a variety of instabilities that have been attributed to the presence of electron and ion beams in the magnetospheric plasma. The auroral electron beam is a prime example of a beam that can give rise to waves at a wide range of frequencies, which will be discussed in detail below. The auroral acceleration process also accelerates ion beams out of the ionosphere that can enhance EIC instabilities. Ion beams accelerated in the tail reconnection region have also been invoked to explain broadband electrostatic noise in the plasma sheet boundary layer. After a brief discussion of these ion instabilities, we will discuss the WKB theory of lower hybrid waves proposed by Maggs (1976) in some detail.

Ion beams have been closely associated with the presence of EIC waves (Kintner et al., 1979) as well as weak double layers (Temerin et al., 1982; Koskinen et al., 1990). Since these ion beams typically have speeds less than the electron thermal speed, they may excite the EIC instability (Recall that for the EIC instability, the electrons are treated as hot, therefore  $\omega / k_{\parallel} a_e \ll 1$ ). A difficulty with the ion-beam driven instability is that the growth due to the ion beam must overcome damping due to the electrons. It has been suggested, however, that the simultaneous presence of electron drifts and ion beams may be particularly unstable (Hauck et al., 1976). This instability is caused by a coupling between the negative energy wave of the ions ( $\omega = k_{\parallel} v_b - \omega_{pb}$ , where  $v_b$  is the ion beam speed and  $\omega_{pb}$  is the plasma frequency of the ion

beam) and the usual EIC wave driven by the drifting electrons. Considering a simple model of the dielectric constant for the EIC waves assuming hot electrons, cold magnetized background ions and an ion beam, we would find:

$$\varepsilon = 1 + \frac{1}{k^2 \lambda_D^2} - \frac{\omega_{pi}^2}{\omega^2 - \Omega_i^2} - \left( \frac{k_{\parallel}}{k} \right)^2 \frac{\omega_{pb}^2}{(\omega - k_{\parallel} v_b)^2} = 0 \quad (119)$$

In the absence of the beam term, this dispersion relation describes the fluid EIC mode. With the beam present, it can be seen that this dispersion relation becomes a fourth order equation such as that found for the two-stream instability.

Another aspect of ion beam interactions is that frequently both hydrogen and oxygen ion beams are observed simultaneously in the auroral zone. If one considers that these ions are accelerated by the same potential drop, these two different beam species should have the same energy. This fact implies that the hydrogen streaming velocity should be 4 times greater than that of oxygen. In fact, this relationship is approximately observed (Collin et al., 1981). However, more careful analysis has revealed that the oxygen beam is frequently more energetic than the hydrogen beam (Collin et al., 1986), with the potential drop as implied by the electron loss cone intermediate between the two beam energies.

These observations can be accounted for by noting that the relative streaming velocity between the hydrogen and oxygen ions can give rise to a two-stream instability (Bergmann and Lotko, 1986; Kaufmann et al., 1986; Dusenbery and Martin, 1987). This instability is directly analogous to the two-stream instability discussed during the first quarter of this course, and, for parallel propagation, may be considered to be the interaction of a slow hydrogen beam mode and a fast oxygen beam mode. Again assuming hot electrons, this dispersion relation can be written for parallel propagation as:

$$\varepsilon = 1 + \frac{1}{k^2 \lambda_{De}^2} - \frac{\omega_{pH}^2}{(\omega - k_{\parallel} v_{bH})^2} - \frac{\omega_{pO}^2}{(\omega - k_{\parallel} v_{bO})^2} = 0 \quad (120)$$

which again leads to a fourth order equation for the frequency that can have complex roots. These modes, however, can also propagate at an angle to the background magnetic field, and in this case, there is also the possibility of coupling to slow and fast cyclotron waves, with frequencies  $k_{\parallel} v_b \pm \Omega_i$  (Bergmann et al., 1988). It is found that the parallel propagating modes dominate for small relative beam speeds, but become stabilized for larger beam speeds, where the oblique modes dominate.

Turning now to electrons, it seems likely that the auroral electron beam could excite a variety of instabilities. Since the beam has an energy much larger than the thermal velocity of the electrons, the most likely modes to be excited are those with phase velocities greater than the electron thermal speed; i.e., those waves in which the background plasma can be considered cold. This suggests that the prime candidates for such excitation would be waves on the upper hybrid and lower hybrid resonance cones, and for multi-ion plasmas, waves near the ion-ion hybrid frequency. (Note that the electron beam speed is usually less than the Alfvén speed, so Alfvén waves can not be excited by Landau resonance.) It should also be noted that although the primary auroral electron beam propagates down the field line, these considerations should also hold for electrons streaming up the field lines such as those recently observed by FAST.

An interesting calculation on these instabilities was performed by Maggs (1976, 1978; see also Lotko and Maggs, 1979; Maggs and Lotko, 1981). Maggs performed a first principles calculation of the wave spectra in the lower and upper hybrid resonance cones by calculating the

thermal fluctuation levels due to the beam, calculating the growth rate, and then determining the total wave amplitude by considering the WKB propagation of the wave in a simple model of the auroral magnetosphere. The calculation is based on the model equation:

$$\frac{\partial P(\omega)}{\partial \omega} = \int dk_{\parallel} \int_{obs}^{\infty} ds E F e^{2M} \quad (121)$$

where  $\partial P/\partial \omega$  is the differential wave power observed per unit frequency,  $E$  is the incoherent wave power due to the Cerenkov emission of the beam,  $F$  is a geometric factor representing the divergence of ray paths and  $M = \int_{obs}^s ds' (\gamma/v_g)$  is the amplification factor that indicates the growth the wave due to the instability. In the second quarter of this course we calculated the incoherent emission due to an unmagnetized beam of particles; a similar calculation for a magnetized plasma yields the expression:

$$E = \frac{q^2}{(2\pi)^3} \int d^3k \sum_{\mathbf{k}} \mathbf{V}_l^* (\mathbf{k}) \cdot \bar{\sigma}^{-1} (\mathbf{k}, k_{\parallel} v_{\parallel} + l\Omega) \cdot \mathbf{V}_l (\mathbf{k}) \quad (122)$$

where  $\mathbf{V}_l \equiv (iv_{\perp} J'_l, (l\Omega/k_{\perp}) J_l, v_{\parallel} J_l)$  is the generalized velocity that was introduced during our discussion of the magnetized dispersion relation. The geometric factor  $F$  can be found by noting that these wave modes are essentially radiated out along a cone (Recall that on the resonance cone the group velocity is perpendicular to the phase velocity, and is just a function of the wave frequency). Thus, we can take  $F = 1/2\pi s_{\perp}$ , where  $s_{\perp}$  is the perpendicular distance between the observer and the wave emission point.

The amplification factor  $M$  is dependent on the propagation characteristics of the wave. Maggs assumed that the auroral electron beam took the form of a sheet, limited in latitudinal size but extended in longitude, following the typical form of the aurora. The wave was assumed to propagate by means of the WKB equations:

$$\dot{\mathbf{x}} = \frac{\partial \omega}{\partial \mathbf{k}} \quad \dot{\mathbf{k}} = -\frac{\partial \omega}{\partial \mathbf{x}} \quad (123)$$

In order to calculate these factors without the need for a detailed model of the plasma, it was assumed that the density and magnetic field scale lengths, which determine how the dielectric constant changes in space, were constant over the ray path. In this limit,  $\dot{\mathbf{k}}$  is constant and the ray path is parabolic. (Note that in the plane perpendicular to  $\mathbf{B}$ , the group velocity is in the same direction as  $\mathbf{k}_{\perp}$ .) Maximum growth is then achieved by considering the ray path that spends the most time in the unstable region; under this geometry, this is a path which enters one side of the unstable region, just grazes the other side of the region, and then exits from the same side it began. If we let  $x$  be the coordinate on the thin side of the region (the latitudinal direction), and  $y$  be the coordinate on the extended side, this parabolic path will have the form  $x = ay^2/2$ , where  $a = (1/k_{\perp}) dk_{\perp}/dy = \dot{k}_{\perp}/(v_{g\perp} k_{\perp})$ . If we let  $d$  be the width of the region, and  $L$  be the distance in the  $y$  direction that the ray propagates from one side of the region to the other, then  $L = \sqrt{2d/a} = \sqrt{2v_{g\perp} k_{\perp} d / \dot{k}_{\perp}}$ . Then the amplification factor can be written in the form  $M \approx (\gamma/v_{g\perp}) 2L = \sqrt{8\gamma^2 k_{\perp} d / v_{g\perp} \dot{k}_{\perp}}$

Propagation out of the unstable region is not the only way in which the wave growth can be stopped. As the wave propagates in the vertical direction, the parallel wave number also changes. This implies that the parallel phase velocity of the wave changes, and so the wave may

become “de-tuned” from the beam. In fact, for lower hybrid waves, as the wave goes to lower altitudes its phase velocity increases, so that it becomes faster than the beam velocity. Roughly speaking, the parallel phase velocity can change on the time scale  $k_{\parallel}/\dot{k}_{\parallel}$ , and so the amplification factor due to this effect can be written as  $M \approx \gamma\beta k_{\parallel}/\dot{k}_{\parallel}$ , where  $\beta$  is a factor of order unity. In practice, the smaller of the two possible amplification factors will determine the amount of wave growth.

Using this simplified model of wave excitation and propagation, Maggs was able to achieve a rather remarkable agreement between the computed and observed power levels. It should be noted that this calculation proceeds totally from first principles, using observed beam parameters and typical scale lengths for the density and magnetic field, and so any similarity with observed results provides a good deal of confidence that the proper physics is being included. A primary result from this work is that the relative amplitude of the spectral peak in the upper and lower hybrid bands is primarily a function of the ratio of electron plasma frequency to gyrofrequency. When this ratio is less than 1, such as occurs at higher altitudes, the lower hybrid band is favored with maximum altitude near  $2\omega_{LH}$ , while at lower altitudes, where  $\omega_{pe} \gg \Omega_e$ , the upper hybrid band is stronger. This altitude dependence is qualitatively similar to observations, since the lower hybrid waves are generally seen at high altitudes while upper hybrid waves are seen mostly in the ionosphere. Another important result of this model is that, except for very strong beams where growth is quite large, the waves propagate out of the unstable region before quasi-linear processes can significantly flatten the beam. This has helped solve a long-standing puzzle of how the auroral electron beam can persist with a positive slope all the way to the auroral zone.

In a multi-ion plasma, there are also waves near the ion-ion hybrid resonance that can be excited in a similar manner. Lysak and Temerin (1983) and Temerin and Lysak (1984) have analyzed these waves using a model based on that of Maggs. It was found that, in this case, the parallel de-tuning effect was primarily responsible for the limitation of wave growth since the group velocity for these waves was primarily parallel to the magnetic field. Two features of the data were noteworthy: first, the waves were very narrow-banded in frequency, and second, the peak amplitudes were similar to those in the lower hybrid band. Both of these features can be explained if the unstable beam region is very narrow ( $\sim 200$  m). The sharp peak arises due to a sharp transition between the two limiting mechanisms. The second feature is a consequence of the fact that the lower hybrid band, which has a larger growth rate than the lower frequency ion hybrid waves, is much more sensitive to the width of the beam than the ion hybrid waves. Thus, narrow beams limit the lower hybrid waves more than the ion hybrid waves, allowing them to reach similar amplitudes despite a lower growth rate.

The damping of these VLF waves or EIC waves at the cyclotron resonance can result in strong ion heating. Since these instabilities grow due to electrons and are damped by the ions, it provides a conduit for the exchange of parallel momentum and energy between the two species. The momentum transfer gives rise to the anomalous resistivity, while the energy transfer will give transverse ion heating that can result in ion conics. EIC waves have the advantage over lower hybrid waves in that they can heat the bulk of the distribution since the perpendicular wavelength is comparable to the thermal ion gyroradius; however, the heating rate is generally lower. This mechanism may be enhanced in downward current regions with downward pointing parallel electric fields, since the electric field will counteract the mirror force, keeping ions in the heating region (Gorney et al., 1985). In such a model, the energy the heated ions achieve is that

which gives them a sufficiently large mirror force to overcome the parallel potential drop, and is independent of the details of the heating mechanism. Such a model appears to be supported by preliminary data from FAST.

Lower hybrid waves have been a prime candidate for the heating of ion conics (Lysak, 1980; Chang and Coppi, 1981). Evidence that VLF hiss can interact with ions was found from S3-3 data by Gorney et al. (1982) who showed that VLF hiss near the lower hybrid frequency sometimes had absorption features due to ion cyclotron damping. However, they concluded that the resulting heating was too little to account for ion conics. Theoretically, the difficulty with lower hybrid wave heating is that these waves generally have a rather long perpendicular wavelength. The resonant contribution to the ion heating rate was given by (4.130) of the second quarter:

$$S_{\perp, res} = -\pi \frac{q^2}{m} \int \frac{d^3 \mathbf{k}}{(2\pi)^3} |\tilde{\Phi}_{\mathbf{k}}|^2 \int d^3 v \sum_l l \Omega J_l^2(k_{\perp} \rho_i) \delta(\omega - k_{\parallel} v_{\parallel} - l \Omega) \left( k_{\parallel} \frac{\partial}{\partial v_{\parallel}} + \frac{l \Omega}{v_{\perp}} \frac{\partial}{\partial v_{\perp}} \right) f \quad (124)$$

Lower hybrid waves typically have  $\omega/k_{\perp} \gg a_i$ , and so have  $k_{\perp} \rho_i \ll \omega/\Omega \sim l$ . At such small values of its argument, the Bessel function factor in (124) becomes small, limiting the ion heating. Thus, it has been stated that a pre-heating mechanism must be required for lower hybrid waves to be effective at heating ions.

However, more recent results both from sounding rockets (LaBelle et al., 1986; Kintner et al., 1992; Vago et al., 1992) and the Freja satellite (Eriksson et al., 1994) show the presence of lower hybrid cavities, i.e., narrow-scale density depletions driven by the ponderomotive force of electron-beam driven lower hybrid waves. These waves are subject to a modulational instability such as that discussed in the second quarter of this course. This instability results in the lower hybrid pump wave decaying to waves with shorter perpendicular wavelength, as we saw in the second quarter. Sotnikov et al. (1978) showed that the lower hybrid wave is susceptible to such an instability when the wave energy density satisfies the condition:

$$\frac{|\tilde{E}|^2}{8\pi n T_e} > 3 \frac{\Omega_i^2}{\omega_{pi}^2} k^2 \lambda_{Di}^2 \quad (125)$$

For such strong waves, the ponderomotive force depletes the background density, which traps the waves increasing the wave energy density, causing a further density depletion. This process intensifies the wave power and decreases the perpendicular wavelength, which enhances the ion heating rate. These heated ions further contribute to the density depletion since they are accelerated up the field line by the magnetic mirror force. These observations may indeed be the “smoking gun” to explain the ion conic formation; however, it is still not clear whether such waves are sufficient to explain all observations of ion conics.

## 2. Cyclotron maser instabilities: Auroral kilometric radiation

Both electrostatic and electromagnetic instabilities can be excited by anisotropies and/or loss cone distributions. As we have seen, there is a strong loss cone feature in the auroral distribution function, and this loss cone is enhanced in the presence of parallel electric fields. In addition, it has been recently noted that the downgoing auroral electron beam becomes “defocused” as it propagates into the magnetic mirror, creating a horseshoe-shaped distribution (Delory et al., 1998). These features give rise to an electromagnetic instability called the cyclotron maser instability which gives rise to radio emission in the 200 kHz range. This

emission is known as auroral kilometric radiation, since it is generated in the auroral zone and has a wavelength the order of a kilometer. This instability depends on an interesting and somewhat surprising relativistic effect, as we shall see shortly.

The auroral kilometric radiation (AKR) was first identified by Gurnett (1974), although it had in fact been seen earlier, as a radio emission propagating outward from the earth into interplanetary space. Gurnett originally termed it terrestrial kilometric radiation (TKR), but its clear association with the aurora has led to the term AKR being the more widely used. These waves were in the frequency range from 50-500 kHz, and were observed mostly over the poles at distances up to 30  $R_E$ . The lack of observations at equatorial latitudes suggested that this wave emission was generated at relatively low altitude ( $<3 R_E$ ) in the auroral zone, since the relatively high plasma frequency in the plasmasphere prevented the waves from propagating through this region. The power in this emission is very high,  $10^9$  Watts, which compares to the  $10^{11}$  Watts carried by the incoming auroral particles. This suggests, first, a very efficient wave production mechanism, and second, that these waves were produced in the so-called "free space" modes, i.e., the (R,X) and (L,O) branches which connect directly to the vacuum light waves. This second conclusion follows since if these emissions had to tunnel from some other branch of the dispersion relation, they would not be expected to have such a high observed wave power. Of these modes, the (R,X) mode is expected to be favored since the electron gyromotion is also right-handed. Indeed, the observed waves are primarily polarized in the extraordinary mode, although ordinary mode waves are also sometimes observed.

These free space modes, as we have seen, have a phase velocity greater than the speed of light, and so it is clear that the Landau resonance is not able to produce these waves. Thus, it is clear that the cyclotron resonances must be involved in their production. As we have seen, in order for the cyclotron resonances to be destabilizing, we must have a positive perpendicular slope in the distribution function,  $\partial f / \partial v_{\perp} > 0$ , such as may occur at the loss cone boundary.

The cyclotron maser instability caused by this loss cone was first described by Wu and Lee (1979) and has been described in detail in a review by Wu (1985). Assume first that  $\omega > \Omega_e \gg \omega_{pe}$ , that  $k_{\perp} \gg k_{\parallel}$ , and that the emission takes place due to the first harmonic. Then the X mode dispersion equation can be simplified by noting that the electric field is polarized perpendicular to both the wave vector and the background magnetic field, and by assuming waves near the cyclotron frequency. Thus, in terms of last quarter's notes on the electromagnetic dispersion relation (equations 1.42 and 1.43), the X-mode can be written as  $n^2 = \epsilon_{xx}$  which becomes:

$$1 - \frac{k^2 c^2}{\omega^2} - \frac{\omega_{pe}^2}{\omega^2} \left[ 1 - \int d^3v \left( \frac{\Omega_e}{v_{\perp}} \frac{\partial f}{\partial v_{\perp}} + k_{\parallel} \frac{\partial f}{\partial v_{\parallel}} \right) \frac{v_{\perp}^2 J_1'^2(\lambda)}{\omega - k_{\parallel} v_{\parallel} - l \Omega_e} \right] = 0 \quad (126)$$

where  $\lambda = k_{\perp} v_{\perp} / \Omega_e$ . The ordinary mode dispersion relation takes on a similar form, but with  $v_{\parallel}^2 J_1'^2(\lambda)$  rather than  $v_{\perp}^2 J_1'^2(\lambda)$  in the numerator. Since  $k_{\parallel}$  is small compared to  $k_{\perp}$ , the parallel derivative term can be neglected, and, using the cold plasma dispersion to calculate the real part of, we can write the growth rate using the usual formula:

$$\frac{\gamma}{\omega} = \frac{\pi^2 \omega_{pe}^2}{4\omega^2} \int dv_{\parallel} \int dv_{\perp} \delta(\omega - k_{\parallel} v_{\parallel} - \Omega_e) \Omega_e v_{\perp}^2 \frac{\partial f}{\partial v_{\perp}} \quad (127)$$

for the extraordinary mode. The ordinary mode has a similar growth rate but with a factor  $v_{\parallel}^2 / c^2$  inserted into the velocity integration.

On first sight, it appears that the growth rate given by (3) is always negative, since an integration by parts on the perpendicular velocity yields

$$\int dv_{\perp} v_{\perp}^2 \frac{\partial f}{\partial v_{\perp}} = - \int dv_{\perp} 2v_{\perp} f < 0 \quad (128)$$

However, there is a way out of this situation. The electrons in the auroral zone which excite this instabilities have kinetic energies the order of a few kilovolts, which is roughly 1% of the rest energy of the electron. At this energy, relativistic effects are usually not considered important. However, the resonance condition in the delta-function of (128) is very sensitive to the exact resonant velocity, and should be written in general as:

$$\omega - k_{\parallel} v_{\parallel} - \frac{n\Omega_e}{\gamma} = \omega - k_{\parallel} v_{\parallel} - n\Omega_e \sqrt{1 - \frac{v^2}{c^2}} = 0 \quad (129)$$

where we have generalized to the  $n^{\text{th}}$  harmonic and written the gyrofrequency based on the rest mass of the electron as  $\Omega_e$ . Note that, in strong contrast to the non-relativistic resonance condition, this resonance condition depends on both  $v_{\parallel}$  and  $v_{\perp}$  through the Lorentz factor  $\gamma$ . In general, this condition represents an ellipse in velocity space. The equation for this ellipse can be found by taking the term with the square root over to the right hand side of the equation and squaring both sides. The result of this algebra is that the resonance condition can be written as:

$$\frac{v_{\perp}^2}{a^2} + \frac{(v_{\parallel} - v_0)^2}{b^2} = 1 \quad (130)$$

where:

$$\frac{v_0}{c} = \frac{N\varpi}{1+N^2} \quad \frac{a^2}{c^2} = \frac{1+N^2-\varpi^2}{1+N^2} \quad \frac{b^2}{c^2} = \frac{1+N^2-\varpi^2}{(1+N^2)^2} \quad (131)$$

and we define  $N = k_{\parallel} c / n\Omega_e$  and  $\varpi = \omega / n\Omega_e$ .

These resonant ellipse appear to be much different from the usual set of resonance lines that we found in the non-relativistic case, which raises the question of how they relate to each other. The non-relativistic limit corresponds to the limit of large index of refraction, i.e.,  $k_{\parallel} c / \omega \gg 1$  and  $k_{\parallel} c / \Omega_e \gg 1$ . In terms of the variables used above, these two conditions are  $N \gg \varpi$  and  $N \gg 1$ , respectively. It can be seen from (131) that under these limits, we have  $v_0/c = \varpi/N$ ,  $a/c = 1$ , and  $b/c = 1/N$ . In usual units, this implies that  $v_0 = \omega / k_{\parallel}$  and  $b = n\Omega_e / k_{\parallel}$ . Thus the resonance ellipse is centered on the phase velocity, extends to the speed of light in the perpendicular velocity direction, and intercepts the parallel velocity axis at  $(\omega \pm n\Omega_e) / k_{\parallel}$ , corresponding to both the positive and the negative  $n$  harmonic. (Note that when we derived (4) we had to square (129), and so each ellipse corresponds to both  $\pm n$ .) Thus, in the vicinity of the parallel velocity axis the resonance ellipse is a straight line at the usual resonance velocity, and the ellipse deviates from a straight line only when  $v_{\perp} \rightarrow c$ . Therefore, our discussion of plasma waves in magnetized plasmas that have parallel phase velocities much less than the speed of light is unaffected.

Waves such as the free space waves considered here have  $\omega / k > c$ , and for nearly perpendicular propagation,  $\omega / k_{\parallel} \gg c$ . Thus here we should take the limit  $N \ll 1$ . In this case, we have  $v_0/c = \varpi N$ , i.e.,  $v_0 = \omega / k_{\parallel}$ , and  $(a/c)^2 = (b/c)^2 = 1 + N^2 - \varpi^2$ , which can also be

written as  $a/c = b/c = \sqrt{k_{\parallel}^2 c^2 + n^2 \Omega_e^2 - \omega^2} / n \Omega_e$ . Thus, if the wave frequency is greater than the gyroharmonic, there must be a finite  $k_{\parallel}$  for the resonance to exist. It is worth noting that in this limit, the resonant ellipse becomes a circle, which can be obtained from the weakly relativistic limit of the resonance condition (129):

$$\omega - k_{\parallel} v_{\parallel} - n \Omega_e \left( 1 - \frac{v^2}{2c^2} \right) = 0 \quad (132)$$

As a sidelight, we may note that in the case  $k_{\parallel} = 0$ , i.e.,  $N = 0$ , such as we have encountered for the Bernstein modes, we stated previously that there was “no cyclotron resonance.” Now it can be seen that in this limit, there are cyclotron resonant circles that are centered at the origin and have a radius in velocity space of  $c \sqrt{1 - \omega / n \Omega_e}$  (Of course, this can only be true for waves just below a gyroharmonic). As far as I know, the consequences of this fact for loss cone instabilities of the electron Bernstein modes have not been considered; however, it can be seen that for weakly relativistic electrons with  $\gamma \sim 1.01$  such as the auroral electrons, this resonance circle is only important for frequencies within 1% of a cyclotron harmonic.

Let us now return to the emission of free space extraordinary mode radiation in the auroral zone. First of all, we note that the frequency of this radiation is greater than the electron gyrofrequency, since the X mode cutoff is given by (equation 3.62 of the first quarter notes):

$$\omega_{R,X} = \frac{1}{2} \left[ \Omega_e + \sqrt{\Omega_e^2 + 4\omega_{pe}^2} \right] \approx \Omega_e \left( 1 + \frac{\omega_{pe}^2}{\Omega_e^2} \right) \quad (133)$$

where the last form gives the low-density limit. In addition, the electrons are only weakly energetic, and so the resonance condition given by (132) for a weakly relativistic plasma applies. This implies we should have a small  $k_{\parallel}$ ; however, we cannot let  $k_{\parallel} \rightarrow 0$  since we must have  $k_{\parallel}^2 c^2 > \omega^2 - \Omega_e^2$  for there to be a resonant ellipse. This same condition implies that we want the frequency to be as close to the gyrofrequency as possible. Considering equation (133), we clearly want the ratio of plasma to gyrofrequency to be as small as possible. Thus, the instability is most effective in a low-density plasma.

Fortunately, the auroral zone provides for such a low-density plasma, since, above the region of parallel electric field, the ionospheric electrons cannot overcome the potential barrier. As noted by Calvert (1981), the density in the auroral zone above the acceleration region can achieve low enough values so that  $\omega_{pe} / \Omega_e \approx 0.05$ . The theory of Wu and Lee (1979) predicts that growth can occur near the electron gyrofrequency whenever  $\omega_{pe} / \Omega_e < 0.3$ . Thus the auroral cavity plays an important role in the formation of AKR. In addition, this localized low-density region can also trap the X mode radiation, since outside the cavity, the plasma density and thus the X-mode cutoff is higher. When the X-mode cutoff outside the region is greater than the wave frequency, the waves are reflected back into the source region and can thus be further amplified.

Recent FAST observations have concluded that the emission of AKR is associated primarily with a horseshoe type distribution rather than the loss cone (Ergun et al., 1998b; Delory et al., 1998). These emissions favor the  $k_{\parallel} \approx 0$  mode, which means that the resonance condition (129) describes a circle in velocity space. The emissions are found just under the electron gyrofrequency, consistent with the relativistic decrease of the gyrofrequency of the energetic electrons.

A final interesting aspect of observed AKR waves is that they are emitted in a series of very narrow-banded bursts (Gurnett and Anderson, 1981; Benson et al., 1988; Menietti et al., 1996) that drift generally downward in frequency, although upward drifts are also sometimes observed. This drift implies that the source region moves up (and sometimes down) the field line, since the wave frequency is closely tied to the electron gyrofrequency. Menietti et al. (1996) suggest that these drifts are associated with the triggering of the AKR by another, low-frequency wave mode that propagates up the field line, such as electromagnetic ion cyclotron waves. As a final point, there have also been ground observations of waves near the harmonic of the electron gyrofrequency observed from the ground, which have been termed “auroral roar” (Kellogg and Monson, 1979; LaBelle et al., 1995). These waves may be generated by a similar mechanism as the cyclotron maser instability, but details of this excitation are still unclear.

### *3. Electron and Ion Phase Space Holes and Solitary Waves*

Current or beam-driven waves in the auroral zone can potentially grow into nonlinear structures, often referred to as phase space holes or solitary waves. Unstable plasma waves will cause fluctuations in the potential along auroral field lines. These fluctuations could grow due to a mechanism suggested by Lotko (1983) for negative polarity ion acoustic soliton. In the presence of a current, a negative potential fluctuation represents a barrier to the flow of electrons, and electrons with an energy (in the hole frame) smaller than the potential barrier will be reflected from the barrier. In the presence of a net drift between electrons and ions, there will be more electrons reflecting from the hole from one side than from the other. Thus, there will be an excess of electrons on one side of the barrier and a deficiency on the other. Therefore, in a procedure much analogous to Landau damping, the hole will gain momentum and grow. In addition, the space charge will lead to a net potential drop across the hole since the side with more electrons will be more negative than the other side. In this way a double layer can form from this ion hole mode.

While the weak double layer model was initially a very promising mechanism for the auroral potential drop, further investigations have cast doubt on this model. Mälkki et al. (1993; see also Koskinen and Mälkki, 1993; Eriksson and Boström, 1993) have investigated the plasma environment of weak double layers on the Viking satellite, and found that most solitary wave structures observed had very little ( $< 1$  V) or no parallel potential drop associated with them, and that both upward and downward potential drops were almost equally likely. The total potential drop inferred from these observations was no more than 1 kV, at the lower end of that necessary to explain auroral acceleration. Nevertheless, such holes are interesting plasma physics objects in their own right.

Both electron (positive potential) and ion (negative potential) holes are found along auroral field lines. FAST results (Ergun et al., 1998) show that ion holes are associated with upward ion beams in the upward current regions, while electron holes are associated with upward electron beams in downward current regions. These results have been confirmed with Polar data by Bounds et al. (1999). These results would indicate that these solitary waves are driven by the beams in these two cases.

The theory of such structures is not yet very well developed. The primary means of describing them theoretically are BGK modes or through computer simulation. Muschietti et al. (1999) have constructed a BGK model for electron holes. This model predicts that the amplitude of the mode should increase with its scale size, in contrast, for example, with the usual ion

acoustic solitons where the reverse is true. They also performed two-dimensional simulations on these structures, showing that they maintained their one-dimensional character despite perturbations in the other direction. These properties are consistent with Polar data of these structures (Cattell et al., 2001). In another approach to dealing with these structures, Goldman et al. (1999) have performed two-dimensional simulations of the nonlinear evolution of the electron-electron two-stream instability, and showed that repetitive hole structures formed in their simulations. In these simulations, however, the holes eventually decayed due to the emission of whistler mode emissions.

Ion hole structures have been also been addressed through simulations. Crumley et al. (2001) have performed simulations based on the ion-ion two-stream instability discussed above. Their results showed that ion holes formed with velocities between the speeds of the hydrogen and oxygen ion beams, consistent with the ion-ion two-stream mechanism. The formation of holes in this case was enhanced by the lack of a cold electron background in the simulations. Thus, this instability and the formation of ion holes would be favored above the auroral potential drop, where they are in fact found, since this potential drop excludes the cold electrons.

### References

- Abramowitz, M., and I. A. Stegun, *Pocketbook of Mathematical Functions*, Verlag Harri Deutsch, Frankfurt am Main, Germany, 1984.
- Alfvén, H., and C.-G. Fälthammar, *Cosmic electrodynamics*, Clarendon Press, Oxford, 1963.
- Arnoldy, R. L., The relationship between field-aligned current carried by superthermal electrons and the auroral arc, *Geophys. Res. Lett.*, *4*, 407, 1977.
- Benson, R. F., M. M. Mellott, R. L. Huff, and D. A. Gurnett, Ordinary mode auroral kilometric radiation fine structure observed by DE 1, *J. Geophys. Res.*, *93*, 7515, 1988.
- Bergmann, R. and W. Lotko, Transition to unstable ion flow in parallel electric fields, *J. Geophys. Res.*, *91*, 7033, 1986.
- Bergmann, R., I. Roth, and M. K. Hudson, Linear stability of the  $H^+O^+$  two-stream interaction in a magnetized plasma, *J. Geophys. Res.*, *93*, 4005, 1988.
- Boehm, M. H., J. Clemmons, and G. Paschmann, Freja observations of a ten-meter boundary within monoenergetic auroral electron precipitation, *Geophys. Res. Lett.*, *22*, 69, 1995.
- Borovsky, J. E., The production of ion conics by oblique double layers, *J. Geophys. Res.*, *89*, 2251, 1984.
- Borovsky, J. E., Auroral arc thicknesses as predicted by various theories, *J. Geophys. Res.*, *98*, 6101, 1993a.
- Borovsky, J. E., The strong double layer model of auroral arcs: an assessment, in *Auroral Plasma Dynamics*, R. L. Lysak (ed.), American Geophysical Union, Washington, p. 113, 1993b.
- Borovsky, J. E., and D. M. Suszcynsky, Optical measurements of the fine structure of aurora arcs, in *Auroral Plasma Dynamics*, R. L. Lysak (ed.), American Geophysical Union, Washington, p. 25, 1993.

- Bounds, S. R., R. F. Pfaff, S. F. Knowlton, F. S. Mozer, M. A. Temerin, and C. A. Kletzing, Solitary potential structures associated with ion and electron beams near 1  $R_E$  altitude, *J. Geophys. Res.*, *104*, 28,709, 1999.
- Brown, R. R., Electron precipitation in the auroral zone, *Space Sci. Rev.*, *5*, 311, 1966.
- Calvert, W., The auroral plasma cavity, *Geophys. Res. Lett.*, *8*, 919, 1981.
- Cattell, C. A., J. Crumley, J. Dombeck, R. Lysak, C. Kletzing, W. K. Peterson, and H. Collin, Polar observations of solitary waves at high and low altitudes and comparison to theory, submitted to *Adv. Space Res.*, 2000.
- Chang, T., and B. Coppi, Lower hybrid acceleration and ion evolution in the supraauroral region, *Geophys. Res. Lett.*, *8*, 1253, 1981.
- Chiu, Y. T., and J. M. Cornwall, Electrostatic model of a quiet auroral arc, *J. Geophys. Res.*, *85*, 543, 1980.
- Chiu, Y. T., and M. Schulz, Self-consistent particle and parallel electrostatic field distributions in the magnetospheric-ionospheric auroral region, *J. Geophys. Res.*, *83*, 629, 1978.
- Collin, H. L., R. D. Sharp, E. G. Shelley, and R. G. Johnson, Some general characteristics of upflowing ion beams and their relationship to auroral electrons, *J. Geophys. Res.*, *86*, 6820, 1981.
- Collin, H. L., W. K. Peterson, and E. G. Shelley, Solar cycle variation of some mass dependent characteristics of upflowing beams of terrestrial ions, *J. Geophys. Res.*, *92*, 4757, 1986.
- Crumley, J. P., C. A. Cattell, R. L. Lysak, and J. P. Dombeck, Studies of ion solitary waves using simulations including hydrogen and oxygen beams, *J. Geophys. Res.*, *106*, 6007, 2001.
- Delory, G. T., R. E. Ergun, C. W. Carlson, L. Muschietti, C. C. Chaston, W. Peria, J. P. McFadden, and R. Strangeway, FAST observations of electron distributions within AKR source regions, *Geophys. Res. Lett.*, *25*, 2069, 1998.
- Dusenbery, P. B., and R. F. Martin, Jr., Generation of broadband turbulence by accelerated auroral ions: 1. Parallel propagation, *J. Geophys. Res.*, *92*, 3261, 1987.
- Eliasson, L., M. André, R. Lundin, R. Pottellette, G. Marklund, and G. Holmgren, Observations of electron conics by the Viking satellite, *J. Geophys. Res.*, *101*, 13,225, 1996.
- Ergun, R. E., C. W. Carlson, J. P. McFadden, F. S. Mozer, G. T. Delory, W. Peria, C. C. Chaston, M. Temerin, I. Roth, L. Muschietti, R. Elphic, R. Strangeway, R. Pfaff, C. A. Cattell, D. Klumpar, E. Shelley, W. Peterson, E. Moebius, and L. Kistler, FAST satellite observations of large-amplitude solitary structures, *Geophys. Res. Lett.*, *25*, 2041, 1998a.
- Ergun, R. E., C. W. Carlson, J. P. McFadden, F. S. Mozer, G. T. Delory, W. Peria, C. C. Chaston, M. Temerin, R. Elphic, R. Strangeway, R. Pfaff, C. A. Cattell, D. Klumpar, E. Shelley, W. Peterson, E. Moebius, and L. Kistler, FAST observations in the AKR source region, *Geophys. Res. Lett.*, *25*, 2061, 1998b.
- Ergun, R. E., C. W. Carlson, J. P. McFadden, F. S. Mozer, and R. J. Strangeway, Parallel electric fields in discrete arcs, *Geophys. Res. Lett.*, *27*, 4053, 2000.
- Eriksson, A. I., and R. Boström, Are weak double layers important for auroral particle acceleration?, in *Auroral Plasma Dynamics*, R. L. Lysak (ed.), Geophysical Monograph 80, American Geophysical Union, Washington, p. 105, 1993.
- Eriksson, A. I., B. Holback, P. O. Dovner, R. Boström, G. Holmgren, M. André, L. Eliasson, and P. M. Kintner, Freja observations of correlated small-scale density depletions and enhanced lower hybrid waves, *Geophys. Res. Lett.*, *21*, 1843, 1994.
- Evans, D. S., N. C. Maynard, J. Troim, T. Jacobsen, and A. Egeland, Auroral vector electric field and particle comparisons, 2. Electrodynamics of an arc, *J. Geophys. Res.*, *82*, 2235, 1977.

- Fraser, B. J., Ionospheric duct propagation and Pc1 pulsation source, *J. Geophys. Res.*, *80*, 2790, 1975.
- Fried, B. D., and S. D. Conte, *The Plasma Dispersion Function*, Academic, New York, 1961.
- Fridman, M., and J. Lemaire, Relationship between auroral electron fluxes and field aligned electric potential differences, *J. Geophys. Res.*, *85*, 664, 1980.
- Fujita, S., Duct propagation of hydromagnetic waves in the upper ionosphere, 2, Dispersion characteristics and loss mechanism, *J. Geophys. Res.*, *93*, 14,674, 1988.
- Fujita, S., and T. Tamao, Duct propagation of hydromagnetic waves in the upper ionosphere, 1, Electromagnetic field disturbances in high latitudes associated with localized incidence of a shear Alfvén wave, *J. Geophys. Res.*, *93*, 14,665, 1988.
- Fukushima, N., Generalized theorem for no ground magnetic effect of vertical currents connected with Pedersen currents in the uniform-conductivity ionosphere, *Rep. Ionos. Space Res. Japan*, *30*, 35, 1976.
- Goldman, M. V., M. M. Oppenheim, and D. L. Newman, Nonlinear two-stream instabilities as an explanation for auroral bipolar wave structures, *Geophys. Res. Lett.*, *26*, 1821, 1999.
- Gorney, D. J., S. R. Church, and P. F. Mizera, On ion harmonic structure in auroral zone waves: the effect of ion conic damping of auroral hiss, *J. Geophys. Res.*, *87*, 10,479, 1982.
- Gorney, D. J., Y. T. Chiu, and D. R. Croley, Trapping of ion conics by parallel electric fields, *J. Geophys. Res.*, *90*, 4205, 1985.
- Greifinger, C., and P. Greifinger, Theory of hydromagnetic propagation in the ionospheric waveguide, *J. Geophys. Res.*, *73*, 7473, 1968.
- Gurnett, D. A., The earth as a radio source: terrestrial kilometric radiation, *J. Geophys. Res.*, *79*, 4227, 1974.
- Gurnett, D. A., and R. R. Anderson, The kilometric radio emission spectrum: relationship to auroral acceleration processes, in *Physics of Auroral Arc Formation*, Geophysical Monograph 25, S.-I. Akasofu and J. R. Kan (eds.), American Geophysical Union, Washington, p. 341, 1981.
- Harel, M., R. A. Wolf, P. H. Reiff, R. W. Spiro, W. J. Burke, F. J. Rich, and M. Smiddy, Quantitative simulation of a magnetospheric substorm, 1, model logic and overview, *J. Geophys. Res.*, *86*, 2217, 1981.
- Hasegawa, A., and C. Uberoi, *The Alfvén Wave*, Technical Information Center, U.S. Department of Energy, 1982.
- Hauck, J. P., H. Böhmer, N. Rynn, and G. Benford, Ion beam excitation of ion-cyclotron waves and ion heating in plasmas with drifting electrons, *J. Plasma Phys.*, *19*, 253, 1976.
- Hughes, W. J., The effect of the atmosphere and ionosphere on long period magnetospheric micropulsations, *Planet. Space Sci.*, *22*, 1157, 1974.
- Jackson, J. D., *Classical Electrodynamics*, Wiley, New York, 1975.
- Johnstone, A. D., and J. D. Winningham, Satellite observations of suprathermal electron bursts, *J. Geophys. Res.*, *87*, 2321, 1982.
- Kaufmann, R. L., G. R. Ludlow, H. L. Collin, W. K. Peterson, and J. L. Burch, Interaction of upgoing auroral H<sup>+</sup>-O<sup>+</sup> beams, *J. Geophys. Res.*, *91*, 10,080, 1986.
- Kelley, M. C., *The Earth's Ionosphere*, Academic Press, Inc., 1989.
- Kellogg, P. J., and S. J. Monson, Radio emissions from the aurora, *Geophys. Res. Lett.*, *6*, 297, 1979.
- Kindel, J. M., and C. F. Kennel, Topside current instabilities, *J. Geophys. Res.*, *76*, 3055, 1971.
- Kintner, P. M., M. C. Kelley, R. D. Sharp, A. G. Ghielmetti, M. Temerin, C. A. Cattell, and P. F.

- Mizera, Simultaneous observations of energetic (keV) upstreaming ions and EHC waves, *J. Geophys. Res.*, *84*, 7201, 1979.
- Kintner, P. M., J. Vago, S. Chesney, R. L. Arnoldy, K. A. Lynch, C. J. Pollock, and T. E. Moore, Localized lower hybrid acceleration of ionospheric plasma, *Phys. Rev. Lett.*, *68*, 2448, 1992.
- Knight, S., Parallel electric fields, *Planet. Space Sci.*, *21*, 741, 1973.
- Koskinen, H. E. J., and A. M. Mälkki, Auroral weak double layers: a critical assessment, in *Auroral Plasma Dynamics*, R. L. Lysak (ed.), Geophysical Monograph 80, American Geophysical Union, Washington, p. 97, 1993.
- Koskinen, H., R. Lundin, and B. Holback, On the plasma environment of solitary waves and weak double layers, *J. Geophys. Res.*, *95*, 5921, 1990.
- LaBelle, J., P. M. Kintner, A. W. Yau, and B. A. Whalen, Large amplitude wave packets observed in the ionosphere in association with transverse ion acceleration, *J. Geophys. Res.*, *91*, 7113, 1986.
- LaBelle, J., M. L. Trimpi, R. Brittain, and A. T. Weatherwax, Fine structure of auroral roar emissions, *J. Geophys. Res.*, *100*, 21,953, 1995.
- Lotko, W., Reflection dissipation of an ion-acoustic soliton, *Phys. Fluids*, *26*, 1771, 1983.
- Lotko, W., and J. E. Maggs, Damping of electrostatic noise by warm auroral electrons, *Planet. Space Sci.*, *27*, 1491, 1979.
- Lyons, L. R., Generation of large-scale regions of auroral currents, electric potentials, and precipitation by the divergence of the convection electric field, *J. Geophys. Res.*, *85*, 17, 1980.
- Lysak, R. L., Electrostatic ion cyclotron turbulence and auroral particle acceleration, Ph.D. Thesis, University of California, Berkeley, 1980.
- Lysak, R. L., Auroral electrodynamics with current and voltage generators, *J. Geophys. Res.*, *90*, 4178, 1985.
- Lysak, R. L., Ion acceleration by wave-particle interactions, in *Ion Acceleration in the Magnetosphere and Ionosphere*, T. Chang (ed.), AGU Monograph 38, American Geophysical Union, Washington, p. 261, 1986.
- Lysak, R. L., Electrodynamics coupling of the magnetosphere and ionosphere, *Space Sci. Rev.*, *52*, 33, 1990.
- Lysak, R. L., Feedback instability of the ionospheric resonant cavity, *J. Geophys. Res.*, *96*, 1553, 1991.
- Lysak, R. L., Generalized model of the ionospheric Alfvén resonator, in *Auroral Plasma Dynamics*, R. L. Lysak (ed.), AGU Monograph 80, p. 121, 1993.
- Lysak, R. L., Propagation of Alfvén waves through the ionosphere, *Phys. Chem. Earth*, *22*, 757, 1997.
- Lysak, R. L., The relationship between electrostatic shocks and kinetic Alfvén waves, *Geophys. Res. Lett.*, *25*, 2089, 1998.
- Lysak, R. L., Propagation of Alfvén waves through the ionosphere: Dependence on ionospheric parameters, *J. Geophys. Res.*, *104*, 10,017, 1999.
- Lysak, R. L., and C. W. Carlson, Effect of microscopic turbulence on magnetosphere-ionosphere coupling, *Geophys. Res. Lett.*, *8*, 269, 1981.
- Lysak, R. L., and C. T. Dum, Dynamics of magnetosphere-ionosphere coupling including turbulent transport, *J. Geophys. Res.*, *88*, 365, 1983.
- Lysak, R. L., and M. K. Hudson, Coherent anomalous resistivity in the region of electrostatic

- shocks, *Geophys. Res. Lett.*, 6, 661, 1979.
- Lysak, R. L., and M. K. Hudson, Effect of double layers on magnetosphere-ionosphere coupling, *Lasers and Particle Beams*, 5, 351, 1987.
- Lysak, R. L., and W. Lotko, On the kinetic dispersion relation for shear Alfvén waves, *J. Geophys. Res.*, 101, 5085, 1996.
- Lysak, R. L., and Y. Song, A three-dimensional model of the propagation of Alfvén waves through the auroral ionosphere: first results, accepted for publication, *Adv. Space Research*, 2001.
- Lysak, R. L., and M. A. Temerin, Generation of Alfvén-ion cyclotron waves on auroral field lines in the presence of heavy ions, *Geophys. Res. Lett.*, 10, 643, 1983.
- Maggs, J. E., Coherent generation of VLF hiss, *J. Geophys. Res.*, 81, 1707, 1976.
- Maggs, J. E., Electrostatic noise generated by the auroral electron beam, *J. Geophys. Res.*, 83, 3173, 1978.
- Maggs, J. E., and W. Lotko, Altitude dependent model of the auroral beam and beam-generated electrostatic noise, *J. Geophys. Res.*, 86, 3439, 1981.
- Mälkki, A., A. I. Eriksson, P.-O. Dovner, R. Boström, B. Holback, G. Holmgren, and H. E. J. Koskinen, A statistical survey of auroral solitary waves and weak double layers, 1., occurrence and net voltage, *J. Geophys. Res.*, 98, 15,521, 1993.
- Mallinckrodt, A. J., and C. W. Carlson, Relations between transverse electric fields and field-aligned currents, *J. Geophys. Res.*, 83, 1426, 1978.
- McFadden, J. P., C. W. Carlson, and M. H. Boehm, Field-aligned electron precipitation at the edge of an arc, *J. Geophys. Res.*, 91, 1723, 1986.
- Menietti, J. D., and J. L. Burch, Electron conic signatures observed in the nightside auroral zone and over the polar cap, *J. Geophys. Res.*, 90, 5345, 1985.
- Menietti, J. D., H. K. Wong, W. S. Kurth, D. A. Gurnett, L. J. Granroth, and J. B. Groene, Discrete, stimulated auroral kilometric radiation observed in the Galileo and DE 1 wideband data, *J. Geophys. Res.*, 101, 10,673, 1996.
- Miura, A., and T. Sato, Numerical simulation of the global formation of auroral arcs, *J. Geophys. Res.*, 85, 73, 1980.
- Mozer, F. S., C. W. Carlson, M. K. Hudson, R. B. Torbert, B. Parady, J. Yatteau, and M. C. Kelley, Observations of paired electrostatic shocks in the polar magnetosphere, *Phys. Rev. Lett.*, 38, 292, 1977.
- Mozer, F. S., C. A. Cattell, M. Temerin, R. B. Torbert, S. Von Glinski, M. Woldorff, and J. Wygant, The DC and AC electric field, plasma density, plasma temperature, and field-aligned current experiments on the S3-3 satellite, *J. Geophys. Res.*, 84, 5875, 1979.
- Muschietti, L., R. E. Ergun, I. Roth, and C. W. Carlson, Phase-space electron holes along magnetic field lines, *Geophys. Res. Lett.*, 26, 1093, 1999.
- Rees, M. H., Auroral ionization and excitation by incident energetic electrons, *Planet. Space Sci.*, 11, 1209, 1963.
- Sato, T., A theory of quiet auroral arcs, *J. Geophys. Res.*, 83, 1042, 1978.
- Scholer, M., On the motion of artificial ion clouds in the magnetosphere, *Planet. Space Sci.*, 18, 977, 1970.
- Seyler, C. E., and J.-E. Wahlund, Theory of nearly perpendicular plasma waves and comparison to Freja satellite observations, *J. Geophys. Res.*, 101, 21,795, 1996.
- Sharp, R. D., R. G. Johnson, and E. G. Shelley, Observation of an ionospheric acceleration mechanism producing energetic (keV) ions primarily normal to the geomagnetic field

- direction, *J. Geophys. Res.*, *82*, 3324, 1977.
- Sotnikov, V. I., V. D. Shapiro, and V. I. Shevchenko, Macroscopic consequences of collapse at the lower hybrid resonance, *Sov. J. Plasma Phys.*, *4*, 252, 1978.
- Southwood, D. J., and W. J. Hughes, Theory of hydromagnetic waves in the magnetosphere, *Space Sci. Rev.*, *35*, 301, 1983.
- Spiro, R. W., P. H. Reiff, and L. J. Maher, Precipitating electron energy flux and auroral zone conductances: an empirical model, *J. Geophys. Res.*, *87*, 8215, 1982.
- Stasiewicz, K., Y. Khotyaintsev, M. Berthomier, and J.-E. Wahlund, Identification of widespread turbulence of dispersive Alfvén waves, *Geophys. Res. Lett.*, *27*, 173, 2000.
- Swift, D. W., On the formation of auroral arcs and the acceleration of auroral electrons, *J. Geophys. Res.*, *80*, 2096, 1975.
- Temerin, M., and R. L. Lysak, Electromagnetic ion cyclotron (ELF) waves generated by auroral electron precipitation, *J. Geophys. Res.*, *89*, 2849, 1984.
- Temerin, M., C. Cattell, R. Lysak, M. Hudson, R. B. Torbert, F. S. Mozer, R. D. Sharp, and P. M. Kintner, The small scale structure of electrostatic shocks, *J. Geophys. Res.*, *86*, 11,278, 1981.
- Temerin, M., K. Cerny, W. Lotko, and F. S. Mozer, Observations of double layers and solitary waves on auroral zone field lines, *Phys. Rev. Lett.*, *48*, 1175, 1982.
- Trakhtengertz, V. Yu., and A. Ya. Feldstein, Quiet auroral arcs: ionospheric effect of magnetospheric convection stratification, *Planet. Space Sci.*, *32*, 127, 1984.
- Vago, J. L., P. M. Kintner, S. W. Chesney, R. L. Arnoldy, K. A. Lynch, T. E. Moore, and C. J. Pollock, Transverse ion acceleration by localized lower hybrid waves in the topside auroral ionosphere, *J. Geophys. Res.*, *97*, 16,935, 1992.
- Vickrey, J. F., R. R. Vondrak, and S. J. Matthews, The diurnal and latitudinal variation of auroral zone ionospheric conductivity, *J. Geophys. Res.*, *86*, 65, 1981.
- Vogt, J., and G. Haerendel, Reflection and transmission of Alfvén waves at the auroral acceleration region, *Geophys. Res. Lett.*, *25*, 277, 1998.
- Wu, C. S., Kinetic cyclotron and synchrotron maser instabilities: radio emission by direct amplification of radiation, *Space Sci. Revs.*, *41*, 215, 1985.
- Wu, C. S., and L. C. Lee, A theory of terrestrial kilometric radiation, *Astrophys. J.*, *230*, 621, 1979.
- Wygant, J. R., A. Keiling, C. A. Cattell, R. L. Lysak, M. Temerin, F. S. Mozer, C. A. Kletzing, J. D. Scudder, A. V. Streltsov, W. Lotko, C. T. Russell, Evidence for kinetic Alfvén waves and parallel electron energization at 5-7  $R_E$  altitudes in the plasma sheet boundary layer, in press, *J. Geophys. Res.*, 2001.